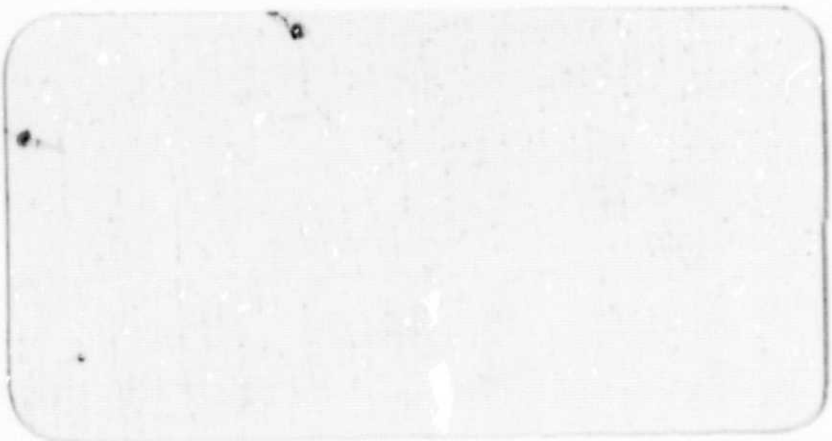

CRinc

THE UNIVERSITY of KANSAS CENTER for RESEARCH, INC.

2291 Irving Hill Drive-Campus West Lawrence, Kansas 66045

MICROWAVE MODEL PREDICTION AND VERIFICATIONS FOR VEGETATED TERRAIN

Prepared for:

NATIONAL AERONAUTICS AND SPACE ADMINISTRATION
LYNDON B. JOHNSON SPACE CENTER
Houston, Texas 77058

Contract NAS 9-15421

Adrian K. Fung

January 1985

Remote Sensing Laboratory
University of Kansas Center for Research, Inc.
Lawrence, Kansas 66045

TABLE OF CONTENTS

Microwave Model Predictions and Verifications for Vegetated Terrain

Abstract

To understand the scattering properties of a deciduous and a coniferous type vegetation scattering models have been developed assuming either a disc-type leaf or a needle-type leaf. The major effort is to calculate the corresponding scattering phase functions and then each of the functions is used in a radiative transfer formulation to compute the scattering intensity and consequently the scattering coefficient. The radiative transfer formulation takes into account the irregular ground surface by including the rough soil surface in the boundary condition. Thus, the scattering model accounts for volume scattering inside the vegetation layer, the surface scattering from the ground and the interaction between scattering from the soil surface and the vegetation volume. The contribution to backscattering by each of the three scattering mechanisms is illustrated along with the effects of each layer or surface parameter. The major difference between the two types of vegetation is that when the incident wavelength is comparable to the size of the leaf there is a peak appearing in the mid angular region of the backscattering curve for the disc-type leaf whereas it is a dip in the same region for a needle-type leaf.

1. Introduction

Existing measurements have indicated that for most mature leafy vegetation scattering is dominated by leaves. This is because stalks are usually partially covered by the leaves and fruits are too few in number and may also be partially covered by leaves. However, when leaves are not present scattering from stalks together with the ground surface is very significant.

In view of the above observations the first step taken in modeling was to examine the scattering effects of leaves. While leaves in real life have many shapes, only the disc-type and the needle-type leaves were modelled and investigated. It should be noted that real leaves are rarely flat and long leaves tend to twist and bend. As a result a large leaf may have more than one scattering centers and hence can be approximated by more than one disc in so far as its scattering properties are concerned. With this understanding it is not truly restrictive to consider only the two types of leaf as stated above.

In the next section major results from the indicated studies are summarized. The derivations and detailed analysis are left in Appendices A and B.

2. Summary of Results

The study of the scattering properties of disc-type leaves was reported by Eom and Fung (1984) before the start of this contract. The major work done on the contract over the past year is to extend previous studies to needle-type vegetation. The detailed development of this study is shown in Appendix A. In addition, a comparison between the scattering properties of the disc-type and the needle-type vegetation was also performed. This study is shown in Appendix B. The major findings are listed below:

(1) For both types of vegetation backscattering is highly dependent on the leaf distributions.

(2) There is a resonant effect for both types of vegetation when the size of the leaf is comparable to the incident wavelength. This causes a dip in the mid angular range of the backscattering curve for the needle-leaf vegetation and a hump for the disc-leaf vegetation.

(3) The resonant effect observed appears in both VV and HH polarizations for the disc-leaf vegetation but only appears in the VV polarization for the needle-leaf vegetation.

(4) The resonance effect is observed in the VH polarization for both types of vegetations.

3. Conclusions

The scattering behaviors of disc-leaf and needle-leaf vegetations have been studied and illustrated in Appendices B. The illustrations include:

(i) The behaviors of the scattering and absorption coefficients as a function of leaf moisture and leaf size.

(ii) The effects of leaf angular distributions on the backscattering coefficients for different polarization states.

(iii) The effects of leaf size and leaf moisture on the backscattering coefficients for different polarization states.

(iv) The frequency dependence of the backscattering coefficients.

(v) The dependence of the backscattering coefficients on soil surface parameters for different polarization states.

(vi) The relative strengths of volume, surface, and volume-surface scattering to the total backscattering coefficient for different polarization states.

In Appendix A the effects of size and orientation of a needle-leaf vegetaton on the backscattering characteristics are illustrated without the presence of a soil background. This is done so that the effects due to leaf size and orientations can be observed without being affected by the background.

Reference

Eom, H.J. and A.K. Fung,A Scatter Model for Vegetation up to Ku-band, Remote Sensing of Environment, Vol. 15, pp. 185-200.

Acknowledgment : This work was supported by NASA Johnson Space Center under Contract NAS9 - 15421

APPENDIX A

Scattering From A Random Layer Embedded With Dielectric Needles

H. J. Eom and A. K. Fung

Abstract

Intensity scattering from a random layer imbedded with small dielectric needles is studied for applications to coniferous vegetation. The phase matrix of a thin needle whose length may be appreciable compared to the incident wavelength is presented.

The effects of needle orientation on scattering is taken into account by averaging the phase function over angles of orientation. The backscattering coefficient from the layer is computed by solving the radiative transfer equation. The effects of operating frequency, orientation and size of a needle on like-and cross- backscattering are demonstrated.

It is found that in backscattering angular trends are mainly controlled by the orientation of the needles.

1. Introduction

A theoretical scatter model for a vegetation layer is an important tool in studying radar backscattering from vegetated terrains. Previous studies of vegetation scatter models were developed using either the field approach (Fung, A.K., 1979; Fung, A.K. and F.T. Ulaby, 1978; Lang, R.H. and J. Sidhu, 1983; L. Tsang and J. Kong, 1981) or the intensity approach (L. Tsang; M. Kubacsi and J. Kong, 1981), (H.J. Eom and A.K. Fung, 1984). In references (L. Tsang; M. Kubacsi and J. Kong 1981),(H.J. Eom and A.K. Fung, 1984), the vegetation layer has been modeled as a random collection of small thin circular discs for applications to leafy vegetation.

In this paper we develop a scattering model for coniferous type vegetation. This means that a vegetation layer is modeled as a random collection of small thin dielectric needles. The phase function of a needle developed under the static assumption (R. Schiffer and K.D. Thielheim 1979) is used in the transfer equation and the backscattering coefficient from such a layer is computed. The effects of frequency, needle size and orientation on backscattering are presented.

In the next section, the phase matrix of a single needle is presented. The angular behavior of the backscattering coefficient is shown in Section 3 for different choices of frequency, needle, size, and orientation. Conclusions are given in Section 4.

2. The Phase Function Of A Single Needle

Consider the scattering problem of a small dielectric needle located at the origin. (See Fig. 1).

From Schiffer and Thielheim (1979), the scattered field is related to the field inside the ellipsoid E_{in} by

$$\vec{E}_s(\vec{r}) = \frac{k^2}{4\pi} \int (\varepsilon_r - 1) \frac{\vec{E}_{in}(\vec{r}')}{r} e^{jk|\vec{r}-\vec{r}'|} d\vec{r}' \qquad (1)$$

where ε_r is the relative permittivity of the needle; k is the wave number in air; and $\vec{r}$, $\vec{r}'$ denote the locations of the field and source points, respectively. According to Stratton (1941), the incident field, $\vec{E}_i = \vec{E}_0 \exp(j\vec{k}_i.\vec{r})$, is related to the field inside the needle-like ellipsoid under static conditions by

$$\vec{E}_{in} = \frac{1}{a_0} \bar{\bar{U}}^{-1} \begin{bmatrix} 1 & 0 & 0 \\ 0 & 1 & 0 \\ 0 & 0 & a_o/a_1 \end{bmatrix} \bar{\bar{U}} \vec{E}_i \qquad (2)$$

$$\triangleq \bar{\bar{A}} . \vec{E}_i$$

where

$$a_0 = 1 + \frac{a^2 c}{2} (\varepsilon_r - 1) A_0 ,$$

$$a_1 = 1 + \frac{a^2 c}{2} (\varepsilon_r - 1) A_1 ,$$

$$A_0 = (c^2-a^2)^{-1} \{c/a^2 + 0.5 (c^2 - a^2)^{-0.5} \ln [\frac{c - (c^2 - a^2)^{1/2}}{c + (c^2-a^2)^{1/2}}]\}$$

$$A_1 = -(c^2-a^2)^{-1} \{(c^2-a^2)^{-0.5} \ln[\frac{c - (c^2-a^2)^{1/2}}{c + (c^2-a^2)^{1/2}}] + 2a\}$$

and a, c are the minor and major semi-axes of the ellipsoid. In

equation (2), the two minor semi-axes of the ellipsoid have been set equal to each other to approximate a circular needle ($c >> a$). According to Schiffer and Thielheim (1979), the static field assumption for E_{in} in equation (1) is valid if $\sqrt{\epsilon_r}\, ka << 1$. Upon substituting equation (2) in equation (1) and specializing to far-zone, we get

$$\vec{E}^{s} \approx (\epsilon_r - 1)\ (k^2/4\pi r)\ e^{jkr}\ \bar{\bar{A}}\ .\ \vec{E}_0 \int \exp[-j(\vec{k}_s - \vec{k}_i)\ .\ \vec{r}']\, d\vec{r}' \tag{3}$$

An evaluation of the integral $\int \exp\,[-j\ \ (\vec{k}_s - \vec{k}_i)\ .\ \vec{r}]\ d\vec{r}'$ is carried out in Appendix A, yielding

$$\bar{E}^{s} \approx \frac{k^2 a^2}{4}\ \ (\epsilon_r - 1)\ \frac{e^{jkr}}{r}\ \ \bar{\bar{A}}.\ \ \bar{E}_0\ \ \frac{\sin\,(0.5\ q_z'\ \ell)}{0.5\ q_z'} \tag{4}$$

where the contents of q_z' and $\bar{\bar{A}}$ are given in Appendix A, and $\ell \approx \frac{4}{3}$ c. The scattering amplitude $\bar{\bar{f}}\ (\vec{k}_s, \vec{k}_i)$ is identified from $\bar{\bar{E}}^{s}$ as (A. Ishimaru 1978)

$$\bar{f}\cdot(\vec{k}_s,\vec{k}_i) = \left[\frac{k^2a^2}{4}(\varepsilon_r-1)\frac{\sin(0.5\,q_z'\,\ell)}{0.5q_z'}\right]$$

$$\begin{bmatrix} (\bar{A}\cdot\hat{v})^T\cdot\hat{v}_s & (\bar{A}\cdot\hat{h})^T\cdot\hat{v}_s \\ (\bar{A}\cdot\hat{v})^T\cdot\hat{h}_s & (\bar{A}\cdot\hat{h})^T\cdot\hat{h}_s \end{bmatrix} \qquad (5)$$

$$\hat{h} = (-\sin\phi,\cos\phi,0)$$

$$\hat{v} = (\cos\theta\cos\phi,\cos\theta\sin\phi,-\sin\theta)$$

$$\hat{h}_s = (-\sin\phi_s,\cos\phi_s,0)$$

$$\hat{v}_s = (\cos\theta_s\cos\phi_s,\cos\theta_s\sin\phi_s,-\sin\theta_s)$$

where the superscript T denotes the transpose of a column matrix. and θandϕ are incident polar and azimuth angles, and θ_s and ϕ_s are scattered polar and azimuth angles (see Fig. 2). The explicit contents of the phase matrix have been defined in terms of the elements of $\bar{f}(\vec{k}_s,\vec{k}_i)$ by Ishimaru (1978).

The phase matrix $\bar{\bar{P}}$ may be constructed as

$$\bar{\bar{P}} = \kappa_e^{-1} n_0 < \bar{\bar{\sigma}} > \qquad (6)$$

where $\bar{\bar{\sigma}}$ is the Stokes matrix expressed in (A. Ishimaru, 1978, p.35) in terms of f_{pq}, the element of $\bar{f}$ given by equation (5); n_0 is the number density of the small ellipsoids; < > denotes averaging over angles α, β and γ to account for the effect of the needle orientation. (See Appendix A for details).

3. Theoretical Angular Behavior of The Backscattering Coefficient

In this section we shall examine the angular behavior of the backscattering coefficient for a random layer embedded with small needles using the phase function derived in the previous sections. The geometry of the scattering problems is depicted in Fig. 2. In

order to solve the backscattering coefficient, the radiative transfer formulation is invoked. A method of solving the transfer equation is available in (H.J. Eom and A.K. Fung 1984); hence, it is not repeated here. To study the angular backscattering behavior of the layer by itself, we assume that the layer has no boundaries. We also assume that the orientation angle α (see Appendix A) is uniformly distributed over $(o, 2\pi)$ such that the layer can be considered to be azimuthally isotropic.

Figures 3-6 show the backscattering coefficients versus the incidence angle for four different choices of needle orientation. The radius and length of the needle are selected to be 0.17 cm and 4 cm, respectively. The frequency is chosen to be 4.5 GHz. Figure 3 shows the behavior when the needles are nearly vertically-oriented. As expected, the level of σ°_{vv} is much higher than that of σ°_{hh}, and the σ°-level increases with the incidence angle θ. Figure 4 depicts σ° when the needles are oriented around 45° off the vertical. Note that both σ°_{vv} and σ°_{hh} show a maximum around 45° incidence angle. Figure 5 shows the case of nearly horizontal orientations. Because of the azimuthally isotropic assumption of the phase function, σ°_{vv} is approximately equal to σ°_{hh} near nadir. As expected, σ°_{vv} drops off much faster than σ°_{hh} as the incidence angle increases. Figure 6 shows σ°_{vv}, σ°_{hh} and σ°_{hv} versus θ when the orientations of needles are assumed to be random. It is seen that random orientations of needles tend to make σ-curves much smoother, relative to the curves shown in Figures 3, 4 and 5.

Figure 7 shows the effects of radar frequency on backscattering. The orientation of needles is assumed to be random. The radius and the length of the needle are chosen to be the same as in Figure 3.

As frequency increases from L to C band, σ_{vv}° and σ_{hh}° drop off faster versus the incidence angle. Note that σ_{vv}° at X-band tends to have a dip around 40°. In order to find out the reason for the dip, it is necessary to investigate the behavior of the phase function given by equation (6). At low frequencies ($k\ell=o$) and under the random orientation assumption σ_{hh}^{0} and σ_{vv}^{0} for a perfectly conducting single needle are

$$\sigma_{hh}^{\circ} \sim \langle |(\bar{\bar{A}} \cdot \hat{h}) \cdot \hat{h}_s|^2 \rangle = 0.24$$

$$\sigma_{vv}^{\circ} \sim \langle |(\bar{\bar{A}} \cdot \hat{v})^T \cdot \hat{v}_s|^2 \rangle = (9 \sin^4\Theta + 15.375 \cos^4\Theta - 7 \sin^2\Theta \cos^2\Theta)/64$$

They are plotted in Fig. 8. Note that σ_{vv}° exhibits a dip. As frequency increases, the effect of the dip on σ_{vv}° is more pronounced due to the presence of $\sin(0.5\, q_z' \ell)/q_z' \ell$. (see Fig. 8 σ_{vv}° for $k\ell=8$). This explains why σ_{vv}° at X-band in Figure 7 retains a slight dip while the others in Fig. 7 do not.

It is important to note that the assumption of random orientation can only guarantee $\sigma_{vv}^{\circ} = \sigma_{hh}^{\circ}$ at normal incidence. At other incidence angles σ_{vv}° may not equal to σ_{hh}° for random orientation because of the lack of symmetry with respect to the incident direction.

Figure 9 depicts the angular behavior of σ° for three different choices of needle size. For the purpose of comparison, the volume of a single needle ($= \frac{4}{3} \pi\ a^2 c$) is kept the same. When the length of the needle (ℓ=2cm and 4cm) is less than the wavelength

(6cm), the difference between σ°_{vv} and σ°_{hh} is not significant. When the length increases to 6cm (about the size of the incidence wavelength), the dip begins to appear in σ°_{vv}.

4. Conclusions

The backscattering coefficients from a random layer embedded with small dielectric needles are computed. The effects of needle orientation and size on backscattering are shown. The scatter model developed in this paper is expected to be useful in the interpretation of radar backscatter from coniferous vegetations at microwave frequencies around X-band or lower.

Appendix A. Scattered Field From A Tilted Dielectric Needle.

The far-zone scattered field from a small tilted needle is (see Figure 1)

$$\vec{E}^s = (\epsilon_r - 1)\frac{k^2}{4\pi r} e^{jkr} \bar{\bar{A}} \cdot \vec{E}_o \int \exp\left[-j\left(\vec{k}_s - \vec{k}_i\right) \cdot \vec{r}'\right] d\vec{r}'$$

where

$$\vec{k}_s - \vec{k}_i = k\left[\left(\sin\theta_s \cos\phi_s - \sin\phi \cos\phi\right)\hat{x} + \left(\sin\theta_s \sin\phi_s - \sin\theta \sin\phi\right)\hat{y} + \left(\cos\theta_s - \cos\phi\right)\hat{z}\right]$$

$$\triangleq (q_1, q_2, q_3) = \vec{q}$$

For convenience, the integration will be carried out in the local coordinate (x", y", z") where the three semiaxes of the needle are aligned with the tilting needle. The local coordinate (x", y", z") is related to the reference coordinate (x,y.z) through the transformation $\bar{\bar{U}}$ containing the three Eulerian angles of orientation,

$$\begin{bmatrix} x'' \\ y'' \\ z'' \end{bmatrix} = \begin{bmatrix} \cos\beta\cos\alpha & \sin\alpha\cos\beta & \sin\beta \\ -(\cos\alpha\sin\beta\sin\gamma + \sin\alpha\cos\gamma) & (-\sin\alpha\sin\beta\sin\gamma + \cos\alpha\cos\gamma) & \cos\beta\sin\gamma \\ (-\cos\alpha\sin\beta\cos\gamma + \sin\alpha\sin\gamma) & -(\sin\alpha\sin\beta\cos\gamma + \cos\alpha\sin\gamma) & \cos\beta\cos\gamma \end{bmatrix} \begin{bmatrix} x \\ y \\ z \end{bmatrix} \quad \text{(A1)}$$

$$\triangleq \bar{\bar{U}}\,[x,y,z]^T$$

where T denotes the transpose of a row vector. Eq. (A-1) is obtained by assuming that the two coordinate systems originally coincide and that an arbitrary orientation of the primed system is achieved by rotating through angles α, β, and γ with respect to the z", y" and x" axes, respectively. Note that the $\bar{\bar{U}}$ matrix is unitary, i.e., $\bar{\bar{U}}^{-1} = \bar{\bar{U}}^{T}$.

Hence
$$\int \exp\left[-j\left(\vec{k}_s - \vec{k}_i\right) \cdot \vec{r}\right] d\vec{r}'$$
$$\underline{\Delta} \int \exp\left[-j\vec{q} \cdot \vec{r}'\right] d\vec{r}'$$
$$= \int \exp\left[-j\bar{\bar{U}} \cdot \vec{q} \cdot \vec{r}''\right] d\vec{r}'' \quad \underline{\Delta} \int \exp\left[-j\vec{q}'' \cdot \vec{r}''\right] d\vec{r}''$$
$$= 2\pi a^2 \frac{\sin\left(q_3'' \ell/2\right)}{q_3''}$$

where a is the radius of the needle and $\ell (\cong \frac{4}{3} c)$ is the length of the needle:

$$q_3'' = U_{31} q_1 + U_{32} q_2 + U_{33} q_3$$

References

Eom, H.J. and Fung, A.K., (1984), "A Scatter Model For Vegetation Up To Ku-band." Remote Sensing of Environment Vol. 15, pp. 185-200.

Fung, A.K. (1979) "Scattering From a Vegetation Layer. IEEE Trans. Geo. Sci. Elect. GE 17, pp. 1-6.

Fung, A.K. and Ulaby, F.T. (1978), "A Scatter Model For Leafy Vegetation IEEE Trans. Geo. Sci. Elect. GE 16, pp. 281-286.

Ishimaru, A. (1978), "Wave Propagation and Scattering in Random Media. Vol. 1. Academic Press, New York.

Lang, R.H. and Sidhu, J. (1983), "Electromagnetic Backscattering From A Layer of Vegetation: A Discrete Approach." IEEE Trans. Geo. Sci. and Rem. Sens. Vol. GE-21, No. 1, pp. 62-71.

Tsang, L. and Kong, J. (1981), "Application of Strong Fluctuation Random Medium Theory to Scattering From Vegetation-Like Half Space." IEEE Trans. Geo. Sci. Remote Sensing GRS-19, pp. 62-69.

Tsang, L., Kubacsi, M., and Kong, J. (1981), "Radiative Transfer Theory for Active Remote Sensing of a Layer of Small Ellipsoidal Scatterers," Radio Science, Vol. 16, pp. 321-329.

Stratton, J.A. (1941), "Electromagnetic Theory." McGraw Hill New York, 1941, pp. 207-213.

Schiffer, R. and Thielheim, K.D. (1979), "Light Scattering by Dielectric Needles and Disks." J. Appl. Phys. Vol. 50, pp. 2476-2483.

Figure Legend

Fig. 1. Geometry of a tilting cylinder. (x,y,z) and (x",y",z") are reference and local coordinates, respectively.

Fig. 2. Geometry of scattering from an inhomogeneous random slab with no bounderies. θ_i, θ_s, and θ_t denote incident, transmitted and scattered angles, respectively.

Fig. 3. Backscattering coefficients versus incidence angle. The orientation of cylinders is assumed to be nearly vertical ($o° < \beta, \gamma < 20°$). ℓ = 4 cm, a = 0.17 cm, f = 4.5 GHz. Volume fraction of scatterer= 0.35%. d= 1.5m, ϵ_r=23+j5

Fig. 4. Backscattering coefficient versus incidence angle. The orientation of cylinders is assumed to be nearly 45° off nadir ($35° < \beta, \gamma < 55°$). ℓ=4cm,a= 0.17 cm,f= 4.5 GHz. Volume fraction of scatterer = 0.35%, d= 1.5m, ϵ_r =23+j5

Fig. 5. Backscattering coefficients versus incidence angle. The orientation of cylinders is assumed to be nearly horizontal. ($70° < \beta, \gamma < 90°$) ℓ = 4 cm, a = 0.17 cm, f = 4.5 GHz. Volume fraction of scatterer = 0.35%, d=1.5m, ϵ_r=23+j5

Fig. 6. Backscattering coefficients versus incidence angle. The orientation of cylinders is assumed to be random. ($0° < \beta < 90°$) ($-90° < \gamma < 90°$) ℓ=4cm a=0.17 cm f= 4.5 GHz

Volume fraction of scatterer= 0.35%, d=1.5m, ϵ_r=23+j5

Fig. 7. The effects of frequency on backscattering. The parameters chosen are the same as those in Fig. 6.

Fig. 8. Illustration of the phase function for a single needle using σ°_{hh} and σ°_{vv}.

Fig. 9. The effects of the size of a cylinder on backscattering. The parameters (β, γ, f, volume fraction, d, and ϵ_r) are the same as those chosen in Fig. 6.

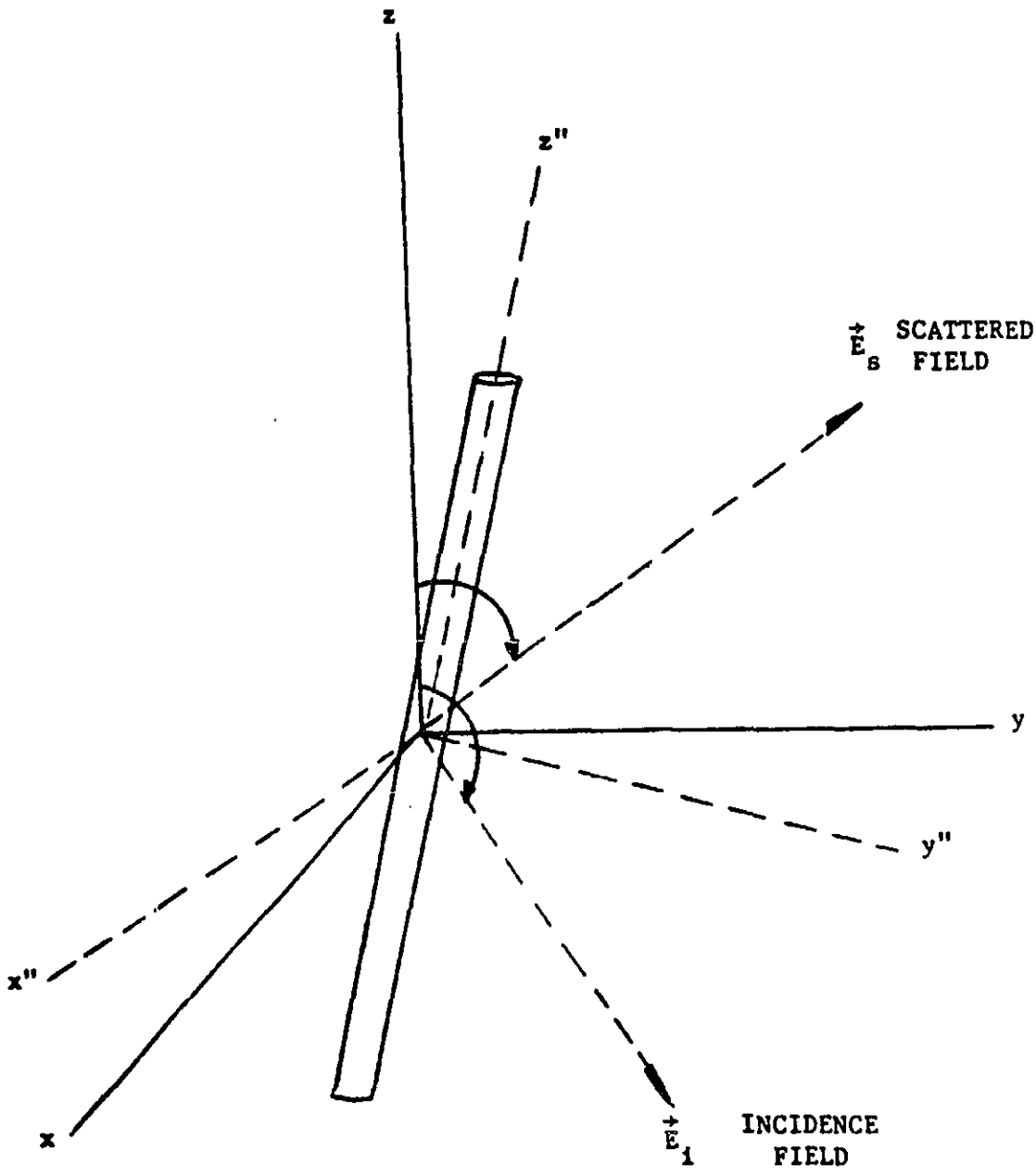
z
z"
$\vec{E}_s$ SCATTERED FIELD
y
y"
x"
x
$\vec{E}_i$ INCIDENCE FIELD

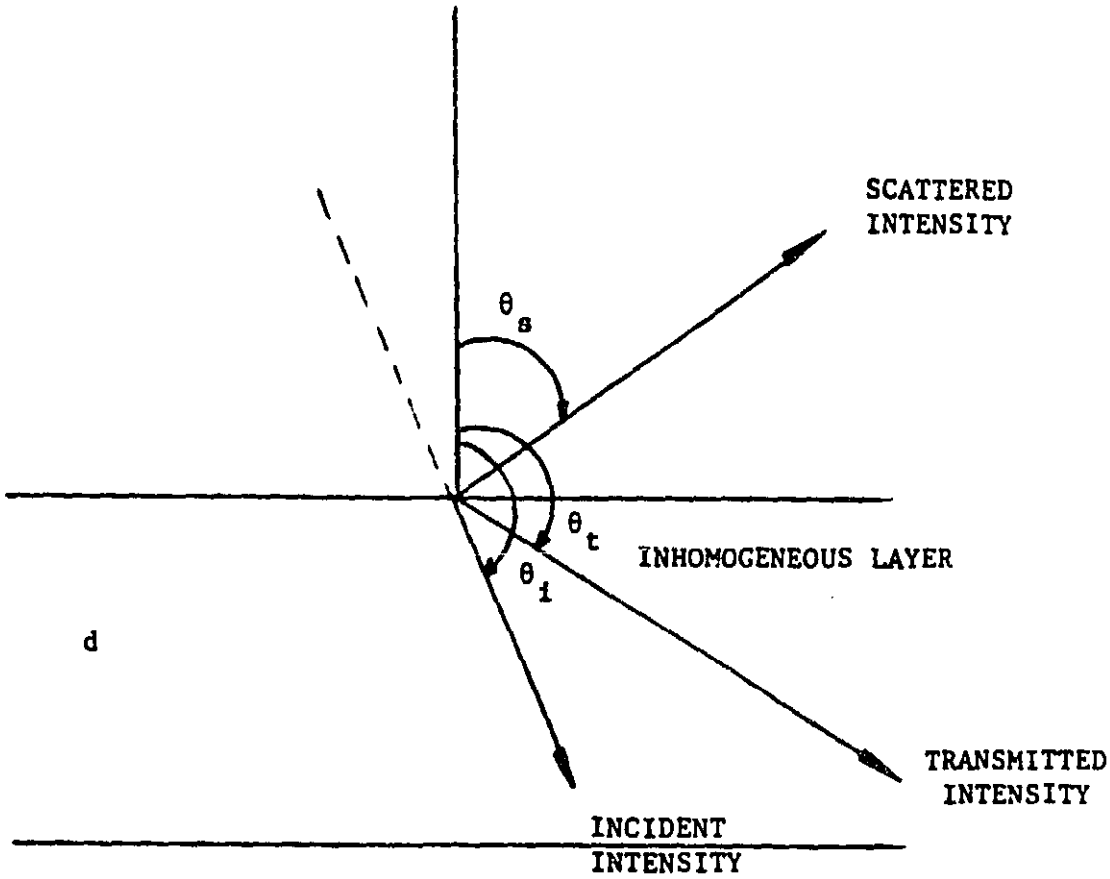
SCATTERED
INTENSITY
θ_s
θ_t
θ_i
INHOMOGENEOUS LAYER
d
TRANSMITTED
INTENSITY
INCIDENT
INTENSITY

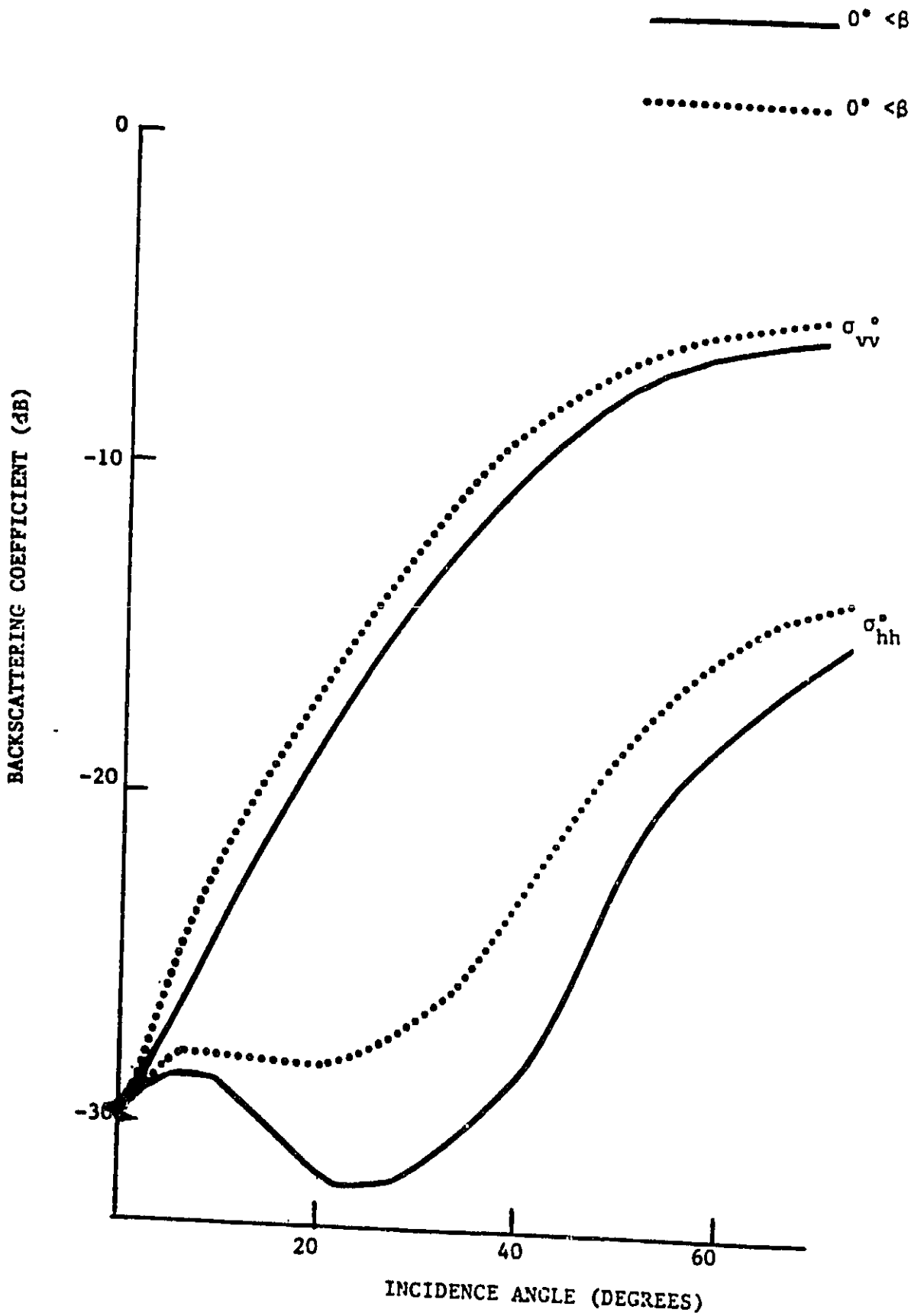
0° <β, γ <10°
0° <β, γ <20°
0
-10
-20
-30
σ°_{vv}
σ°_{hh}
BACKSCATTERING COEFFICIENT (dB)
20
40
60
INCIDENCE ANGLE (DEGREES)

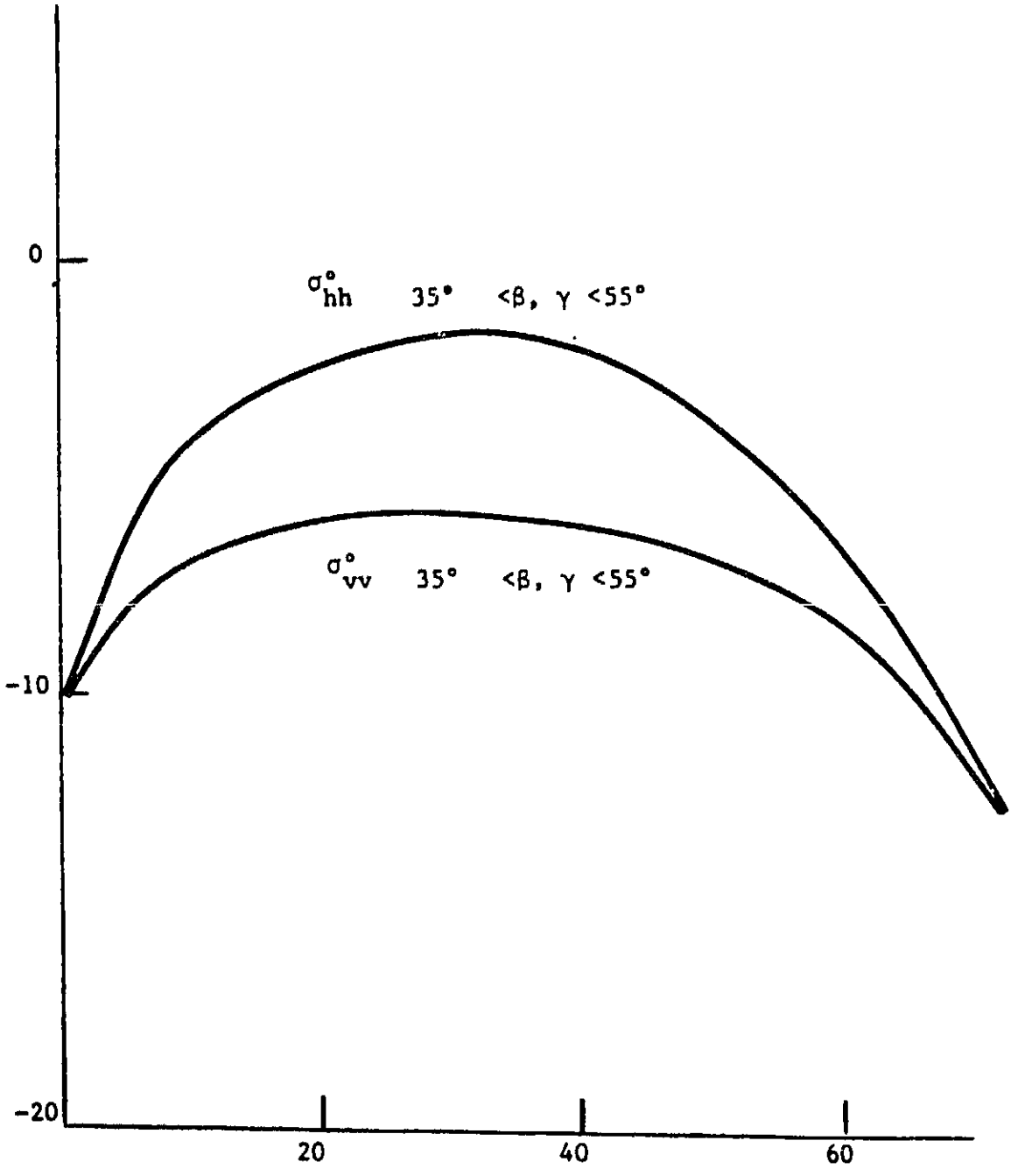
0
-10
-20
σ°_{hh} 35° <β, γ <55°
σ°_{vv} 35° <β, γ <55°
20
40
60
BACKSCATTERING COEFFICIENT (dB)
INCIDENCE ANGLE (DEGREES)

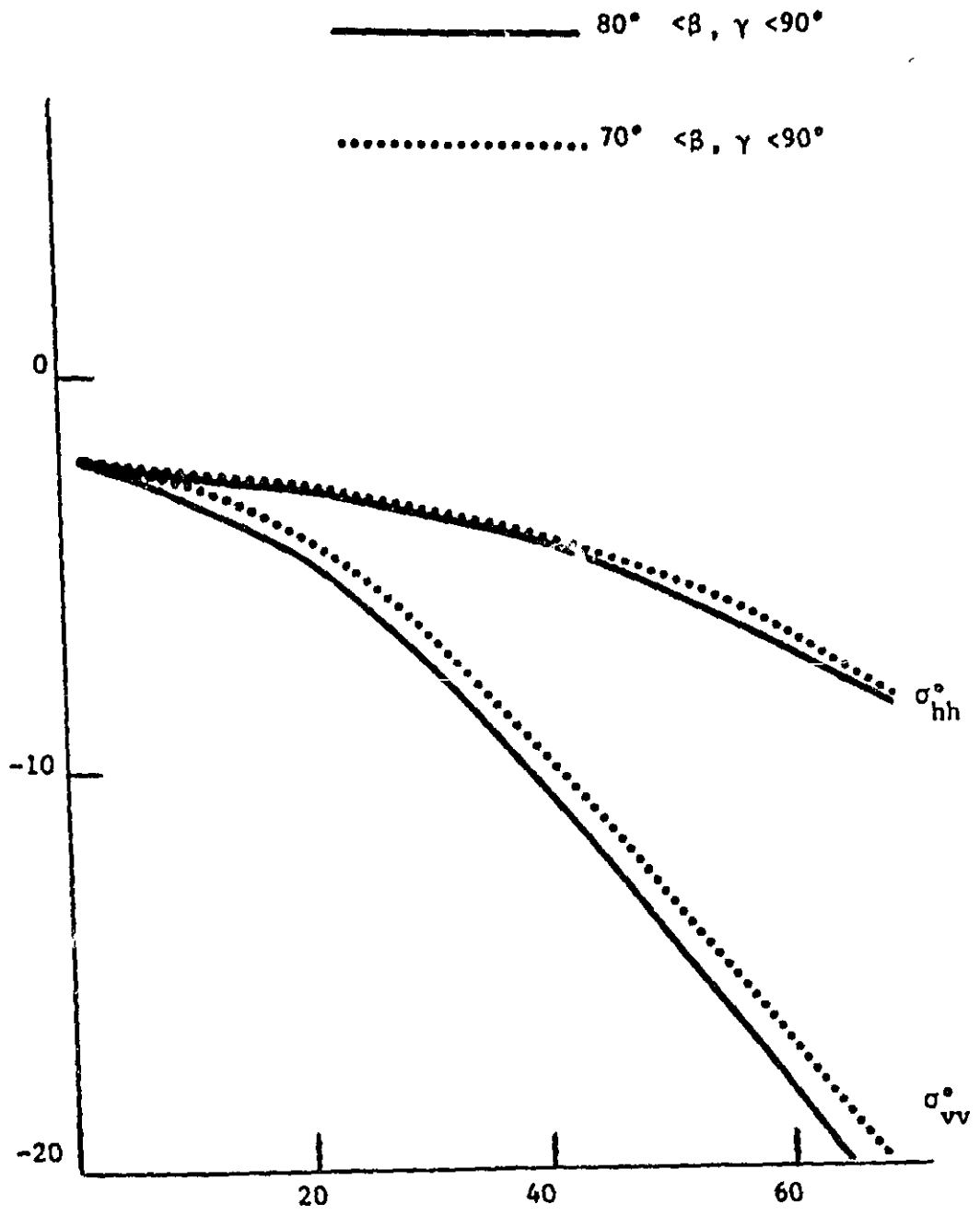
80° <β, γ <90°
70° <β, γ <90°
0
-10
-20
20
40
60
σ°_{hh}
σ°_{vv}
BACKSCATTERING COEFFICIENT (dB)
INCIDENCE ANGLE (DEGREES)

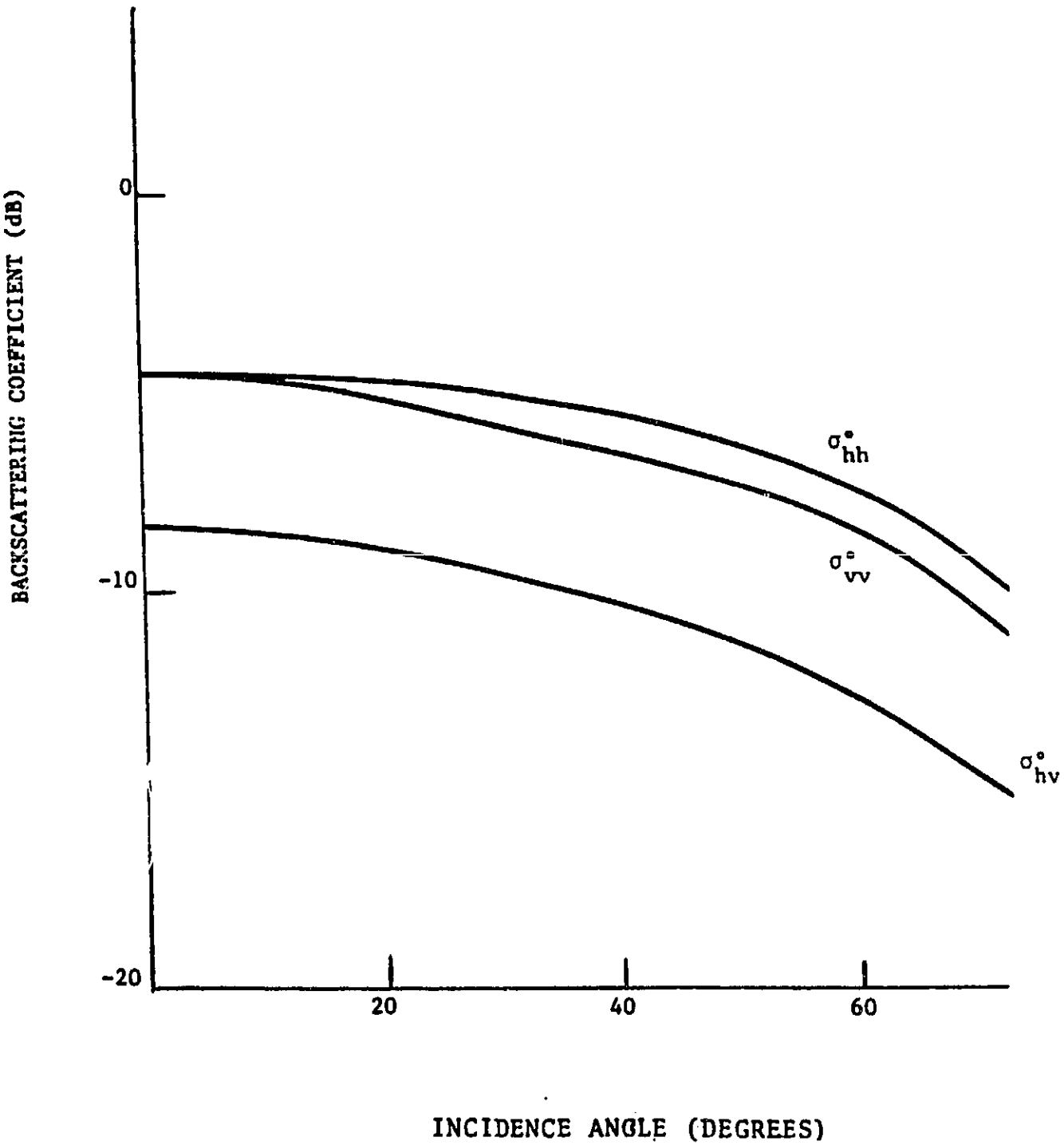
BACKSCATTERING COEFFICIENT (dB)
0
-10
-20
σ°_{hh}
σ°_{vv}
σ°_{hv}
20
40
60
INCIDENCE ANGLE (DEGREES)

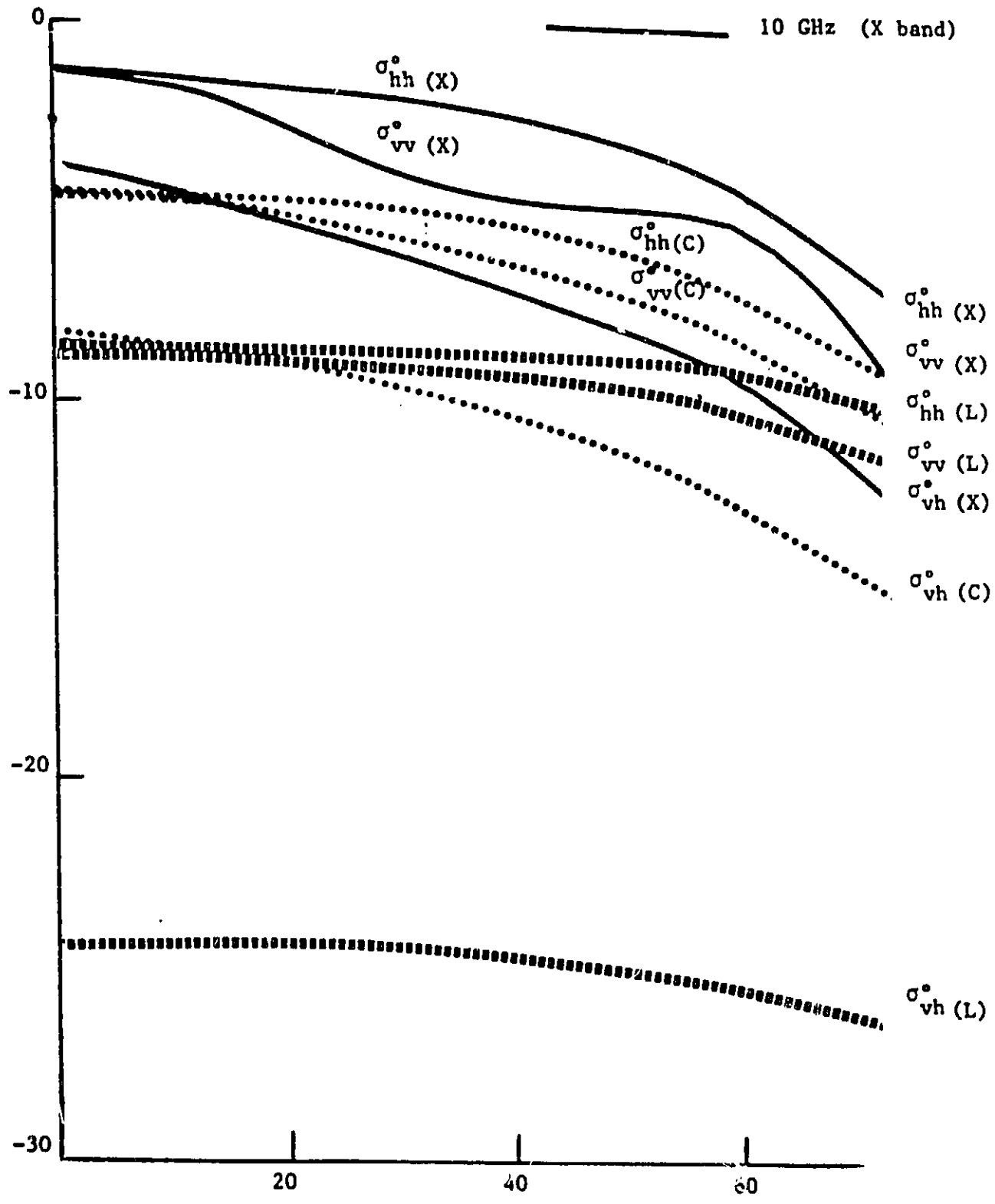

BACKSCATTERING COEFFICIENT (dB)

INCIDENCE ANGLE (DEGREES)

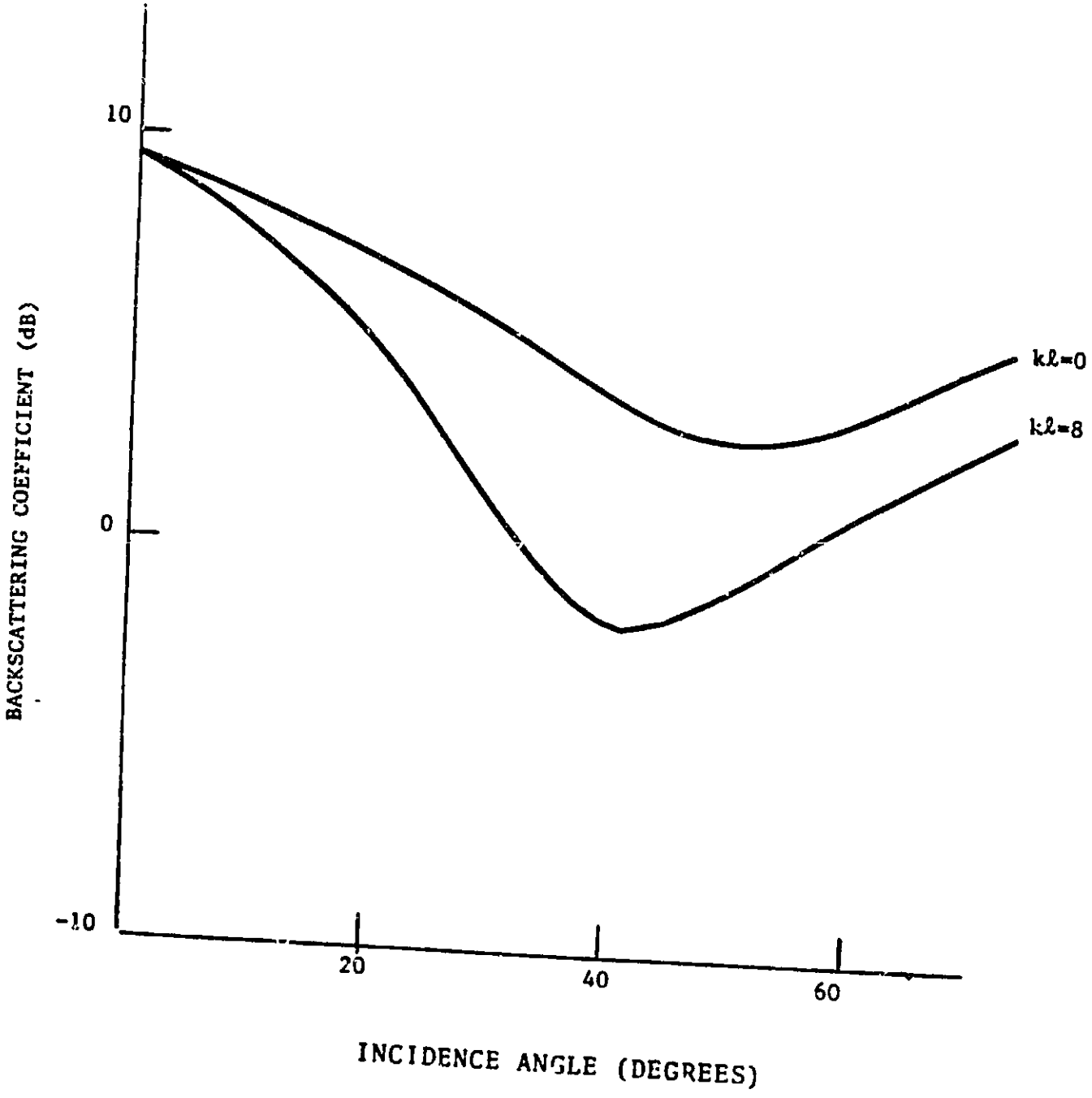
10
0
-10
20
40
60
kℓ=0
kℓ=8
BACKSCATTERING COEFFICIENT (dB)
INCIDENCE ANGLE (DEGREES)

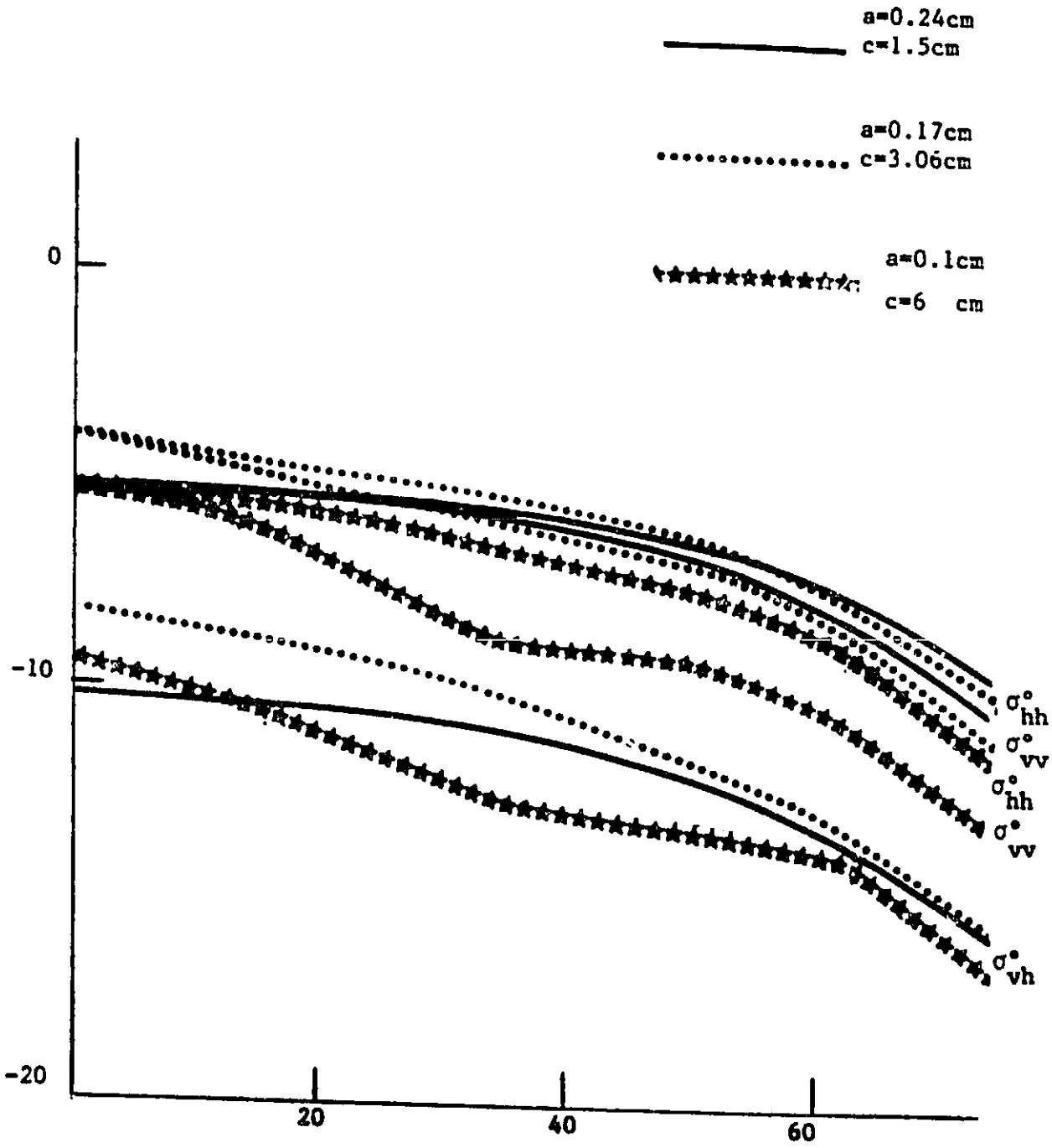
a=0.24cm
c=1.5cm
a=0.17cm
c=3.06cm
a=0.1cm
c=6 cm
0
-10
-20
20
40
60
σ°_{hh}
σ°_{vv}
σ°_{hh}
σ°_{vv}
σ°_{vh}
INCIDENCE ANGLE (DEGREES)

APPENDIX B

PARAMETER EFFECTS IN SCATTERING FROM A VEGETATION LAYER

by

A. K. Fung and H. J. Eom

Abstract

A backscattering model for a layer of vegetation above an irregular ground surface is used to study the effects of vegetation parameters, soil surface parameters, and the interaction between soil and vegetation on backscattering. In addition, the dependencies of model parameters such as the absorption and scattering coefficients and the single scattering albedo on leaf size and leaf moisture are also illustrated. In backscattering calculations the effects of polarization and frequency are also shown.

1. INTRODUCTION

Scattering models for vegetation have been developed by many investigators [1-10]. The vegetation medium is treated either as a continuous random medium [1-5] or as a discrete random medium [6-10]. In the latter case it is easier to correlate model parameters with ground truth parameters. However, most of the discrete approaches are restricted to low frequency applications. More recently, a model [10] using the discrete approach has been generalized to permit wider range of validity in frequency. Hence, this model will be selected for use in the sensitivity studies in this report. Since the details on the computation of the backscattering coefficient and the phase function for a dielectric disc are available in [10], only a dielectric model for a single leaf which is used to relate frequency, volume fraction, leaf moisture, and the density ratio of water to the solid material of the leaf is given below. Other dielectric models are available in [11, 12].

The permitivity of a single leaf is

$$\mathrm{Re}(\varepsilon) = 5.5 + \frac{\varepsilon_m - 5.5}{1 + (1.85/\lambda)^2}$$

$$\mathrm{Im}(\varepsilon) = (\varepsilon_m - 5.5)\frac{(1.85/\lambda)}{1 + (1.85/\lambda)}$$

where $\varepsilon_m = 5 + 51.56\ Vm$

$$Vm = \frac{M}{\frac{dw}{ds} + M\left(1 - \frac{dw}{ds}\right)}$$

In the expressions above λ is the free space wavelength, Vm is the volume fraction of water in the leaf, M is the moisture content ds is the density of the solid material of a leaf, and dw is the density of water.

In the next section the effects of vegetation parameters in the scattering model are illustrated. In addition, the relations between these parameters and leaf size and leaf moisture are also shown. The effects of soil parameters such as soil permitivity and soil surface roughness are discussed in Section 3. In addition, Section 3 also shows the effects of soil and surface interaction by illustrating the relative contributions of the volume-, surface-, and the interaction-terms to total backscattering from a vegetation layer. In Section 4 parameter effects on backscattering from a vegetation layer with needle-shaped leaves are discussed. Ground surface effects and surface-volume interactions are expected to remain the same for this type of vegetation. Conclusions are given in Section 5.

2. VEGETATION PARAMETER EFFECTS.

In the radiative transfer formulation of a scattering model the theoretical parameters are the scattering albedo and the optical thickness. These parameters may also be described in terms of the volume scattering coefficient k_s, the absorption coefficient k_a, and the physical depth of the medium. Both k_s and k_a depend upon the size of the scatterer, its dielectric property, and frequency [10] and hence are directly related to ground truth measurements. For example, the dielectric constant of the leaf is dependent on its moisture content. Thus, the variations of albedo, absorption and scattering coefficients can be plotted directly versus the moisture content in the leaf. This is shown in Fig. 1 for a circularly shaped leaf at 8.6 GHz. It is interesting to note that while all three parameters increase with moisture as expected, the rate of increase for the scattering coefficient is the largest among them. This explains why albedo increases rather slowly with the moisture. Fig. 2 shows these three parameters again as functions of the radius of the circular leaf. All three parameters increase as the radius increases. Here again the scattering coefficient has the largest rate of increase and albedo has the slowest rate of increase. Knowing the dependence of the scattering model parameters on leaf size and leaf moisture, we are now ready to examine the dependence of the backscattering coefficient on these two parameters as well as on leaf angular distributions and frequency.

In Fig. 3 the effects of leaf distributions are shown for both VV and HH polarizations. Three cases are considered: nearly horizontal, nearly vertical, and randomly distributed. When the leaf angular distribution is such that most leaves are lying nearly parallel to the horizontal plane, the vertically polarized field will not be able to excite as much current on the leaves as the horizontally polarized field when the incidence angle is large. Hence, the horizontally polarized scattering coefficient is higher than the vertically polarized coefficient at large angles of incidence. When the leaves are more nearly vertically distributed, the vertically polarized field is able to excite more current and the difference between the two polarizations becomes much smaller. In addition, the backscattering angular curves are almost flat at small angles of incidence and begin to rise at large angles of incidence after experiencing a small dip in the mid angular region. This rise is in agreement with intuition, since more energy can be intercepted by the leaves when the incidence is near grazing. It is interesting to note that when the leaves are randomly distributed the scattering curves do not drop off monotonically as the incidence angle increases. Instead, there is a gradual rise in the mid angular region before the angular drop-off occurs. This unexpected behavior is due to some resonance phenomenon as the size of the leaf approaches a wavelength. This effect is illustrated in Fig. 4 where backscattering coefficients are plotted versus angle of incidence for different leaf sizes under the assumption of random orientation. Note that when the leaf size is small the scattering coefficients for VV and HH are essentially the same and are monotonically decreasing with the incidence angle. On the other hand as the leaf size increases, a gradually more pronounced peak appears in the mid angular region due to the resonance phenomenon.

As we noted in Fig. 1, the effect of increasing moisture is to strengthen scattering. In general, we expect an increase in the level of scattering with moisture. In Fig. 5 we see that while our general expectation holds true the increase is greater for the cross polarized scattering than for the polarized scattering. It is also clear that the level increase is the same for both VV and HH polarization.

In Fig. 6 backscattering at three different frequencies are shown for like and cross polarizations. The scattering curves indicate an increase in the level of scattering at large angles of incidence as frequency increases. This is the expected behavior when volume scattering is dominant. It also follows from the fact that the scatterer becomes larger relative to wavelength as frequency increases. At small angles of incidence polarized scattering reverses its trend with frequency. This is because at near vertical incidence surface scattering from the ground is the dominant contributor to total scattering. It is interesting to note that the increase in scattering is much faster in the L to C band region than the C to X band region. This trend is in agreement with scattering from agricultural crops [10, 13].

3. SOIL PARAMETER EFFECTS AND SURFACE VOLUME INTERACTION

In this section soil surface roughness parameters and soil permitivity changes on the backscattering coefficient of different polarization states are examined. It is known that a larger value of ground moisture gives rise to a larger value of soil permitivity [11, 14]. Hence, the study of permitivity changes is equivalent to that of moisture changes. As may be expected, a larger permitivity causes a stronger surface scattering and leads to a larger backscattering at near vertical incidence. This is illustrated in Fig. 7. It is seen that the effect is significant only at small angles of incidence because at larger incidence angles scattering becomes gradually dominated by volume contributions from the vegetation layer.

Surface roughness effects on backscattering are shown in Fig. 8, where the surface standard deviation is varied by a factor of nine. In addition, contributions to total scattering from soil surface attenuated by the vegetation layer, from vegetation layer alone, and from surface-volume interaction are also shown in the figure. It is seen that as surface roughness increases surface scattering and surface-volume interaction increase. In particular, because of surface-volume interaction the effect of surface scattering propagates to larger angles of incidence. This makes it possible to observe soil moisture dependence at large angles of incidence which might be desirable under special circumstances.

In Fig. 9 polarization dependence of the surface, volume, and surface-volume interaction contributions to total scattering is illustrated. The most significant point to note is that the surface-volume interaction term drops off much faster with the incidence angle for the VV than for the HH polarization. This is because of the Brewster angle effect. Hence, surface scattering effects cannot propagate to large angles of incidence through the surface-volume interaction term in VV polarization for most soil surfaces. In Fig. 9c similar calculations are performed for the cross polarized scattering coefficient. It is seen that because both surface-volume interaction and cross polarized scattering from the layer volume are the result of multiple scattering, the surface volume interaction contribution may be comparable to that of volume scattering contribution. This means that the surface volume interaction contribution is much more important to cross polarized than polarized scattering.

4. PARAMETER EFFECTS OF NEEDLE-SHAPED VEGETATION

In the previous two sections the parameter effects of vegetation with disc-shaped leaves are presented. Vegetations may also be of coniferous type. Hence, it is of interest to study the parameter effects of the needle-shaped vegetation. The detailed development of the scattering model has been given in [15]. The theoretical model parameters are the absorption and scattering coefficients and the medium albedo same as in the disc model. In most practical situations the needles are thin compared to the incident wavelength. Thus, only the variations in the length of the needle is of interest. In Fig. 10 and 11 the dependencies of these three model parameters on the moisture in the needle and the length of the needle are illustrated. In comparison to similar illustrations for disc-shaped leaves the trend behaviors of the model parameters are the same. While the levels of the scattering and absorption coefficients are lower than those shown in Figs. 1 and 2, there is no common basis for making this comparison.

The dependence of the backscattering coefficient on the angular distributions of the needle-shaped leaves is illustrated in Figs: 12 through 15. Four cases are considered. Nearly vertical, nearly horizontal,

around 45° and randomly oriented. When the needles are nearly vertically oriented, there is very little attenuation at normal incidence. The ground scattering is strong at small angles of incidence. As shown in Fig. 12, volume scattering is not important until the incidence angle is larger than 30° for VV polarization and 40° for HH polarization. The cross polarized scattering being dominated by multiple scattering within the inhomogeneous layer is very small at near normal incidence and rises in level fairly quickly as the incidence angle increases. Upon comparing the total scattering for VV and HH polarizations versus corresponding volume scattering by the layer, it is again apparent that the contribution by the surface-volume interaction mechanism is significant for HH polarization but not for VV polarization. Fig. 13 provides similar illustration when the needles are more nearly horizontally distributed. In this case the attenuation due to the layer is very significant and the surface scattering contribution is negligible. Thus, there is practically no difference between the total scattering and volume scattering from the layer. As a result volume scattering curves are not shown on the figure. This large attenuation is the result of the choice of large needle radius and the volume fraction. In Fig. 14 the needles are assumed to distribute around 45°. Here, surface scattering contributions are seen to be dominant at near vertical incidence. When the incidence angle is larger than 10°only volume scattering is important. All the scattering curves, VV HH, and VH, have a hump in the mid angular region. This is clearly due to the assumed needle distribution. In Fig. 15 random distribution is assumed for the needles. Attenuation by the layer is large and surface scattering contribution can be seen only at near normal incidence. Scattering curves for all polarizations decrease monotonically with the incidence angle.

To study the effect of change in needle size on scattering, two approaches are taken: (1) change the length of the needle while its volume is kept constant, and (2) change the length of the needle while other parameters remain constant. The first case is illustrated in Fig. 16. As the needle length increases the angular scattering curves drop off increasingly faster with the incidence angle. This behavior is expected since longer

length implies longer correlation. What is unexpected is that when the needle length approaches one wavelength the VV and VH polarization shows resonant scattering characteristics but HH polarization does not. Case (2) is illustrated in Fig. 17. Here again only VV and VH and polarization show resonant behavior. In comparison with Fig. 4 where the effects of the disc-shaped leaf are shown, it is noted that under resonant condition there is a peak in the mid angular region for the VV scattering coefficient when the leaf is disc-shaped and the reverse is true when the leaf is needle-shaped.

The frequency behavior of a vegetation layer with needle-shaped leaves is shown in Fig. 18. In comparison with Fig. 6 where the disc-shaped leaves are shown, it is seen that volume scattering again increases with the incident frequency. The resonant behavior is not apparent in Fig. 6 after surface scattering contribution is added to the corresponding case in Fig. 3. However, in Fig. 18 the resonant effect is obviously present at 10 GHz for VV polarization. It is interesting to note that the resonant effect is much less pronounced in VH polarization than in VV polarization and can hardly be detected in Fig. 18. The change in level as frequency changes from L to C band is much larger than that when frequency is changed from C to X band. This dependence is the same as observed for disc-shaped vegetation.

For ease of reference the parameter values used in the figures above are tabulated in Tables 1 and 2.

5. CONCLUSIONS

The effects of vegetation and soil parameters on backscattering from vegetation layers with disc-shaped and needle-shaped leaves have been examined. Most of the observed variations are in agreement with intuition but there are several unexpected characteristics also. These are listed below:

1. When the size of the leaf is comparable to the incident wavelength resonance phenomenon is observed in VV and HV polarization for the vegetation with needle-shaped leaves. For disc-shaped leaves resonance appears in all polarization states, VV, HV, and HH.

2. When resonance is observed, a peak appears in the mid angular region for the disc-shaped vegetation and a dip appears for the needle-shaped vegetation.

3. The overall level of scattering for the needle-shaped vegetation is higher than the disc-shaped when volume scattering is dominating. This is not in agreement with measurements. Apparently, the volume fraction was selected at too high a level for the needle-shaped vegetation. The radius of the needle used in the figures is also too large from the practical standpoint.

4. The choice of a disc-shaped leaf with a=1.5 cm and c=0.02 cm and a needle-shaped leaf with a=0.15 cm and c=3.06 cm was made so that both leaves have the same volume. This was done to permit some basis for comparison between the two different types of vegetation. However, this makes the amount of layer attenuation for needle-shaped vegetation much higher than in a practical situation.

As noted in the above statement the level and the amount of attenuation of the needle-shaped vegetation layer are not representative of most real life conditions. However, the trend behaviors should be correct and the parameter effects should be useful for indicating a proper choice of polarization, frequency and incidence angles in experiment design.

References

1. Fung, A. K. and Fung, H. S., Application of first-order renormalization method to scattering from a vegetated-like half-space, IEEE Trans. Geo.Sci.Electr. GE-15:189-195. (1977)

2. Fung, A. K., and Ulaby, F. T., A scatter model for leafy vegetation, IEEE Trans.Geo.Sci. Electr. GE-16:281-286. (1978)

3. Fung, A. K. "Scattering from a vegetation layer," IEEE Trans. Geo. Sci. Electr. GE-17:1-6. (1979)

4. Zuniga, M., Habashy, T., and Kong, J. Active remote sensing of layered random media, IEEE Trans.Geo. Sci.Electr. GE-17:296-302. (1979)

5. Tsang, L., and Kong, J. Application of strong fluctuation random medium theory to scattering from vegetation-like half-space, IEEE Trans. Geosci. Remote Sensing GRS-19:62-69. (1981)

6. Tsang, L., Kubacsi, M., and Kong, J. Radiative transfer theory for active remote sensing of a layer of small ellipsoidal scatterers, Radio Science 16:321-329. (1981)

7. Lang, R. H. Electromagnetic backscattering from a sparse distribution of lossy dielectric scatters, Radio Science, 16:15-30. (1981)

8. Lang, R. H. and Sidhu, J. "Electromagnetic Backscattering from a layer of vegetation: a discrete approach." IEEE Trans. Geo. Sci. and Rem. Sens. Vol. GE-21, No. 1, pp. 62-71. (1983)

9. Ulaby, F. Vegetation clutter model, IEEE Trans. Ant. Prop. AP-28:538-545. (1980)

10. Eom, H. J. and A. K. Fung. "A Scatter Model for Vegetation up to Ku-band." Remote Sensing of Environment Vol. 15, pp. 185-200 1984.

11. Calwell, R. N. "Manual of remote sensing." 2nd ed. Chapter 4, American Soc. Photogrammetry, 1983

12. Hasted, J. B. "Agneous dielectrics" Halsted Press, 1973.

13. Dobson, C., Stiles, H., Brunfeldt, D. Metzler, T., and McMeekin, S. "Data documentation: 1975 MAS 1-8 and MAS 8-18 vegetation experiments,"RSL TR 264-15, Remote Sensing Laboratory, University of Kansas Center for Research, Inc., 2291 Irving Hill Drive, Lawrence, KS 66045. (1977)

14. Wang, J. R., and T. J. Schmugge,"An empirical model for the complex dielectric permittivity of soils as a function of water content," IEEE Trans. Geoscience Remote Sensing Vol. 18, pp 288-295, 1980

15. Eom, H. J. and A. K. Fung,"Scattering from a random layer embedded with dielectric needles,"Electrical Engineering Dept. Wave Application Center, TR 3601-84-1, University of Texas at Arlington, Arlington, TX 76019. Oct. 1984.

Table 1

Parameter For Disc-Shaped Vegetation

Figures	Surface Parameters	β, γ	A & C (cm) Shape	Freq. GHz	Vol. Fract. (%)	Plant Mois. (%)	Physical Depth d & Ground ε_g
Fig 1		0° <β< 90° 0° <γ< 90°	a=1.5cm c=0.02cm Disc	8.6GHz	0.3%	20% 45% 75%	d=1.5m
Fig. 2		0° <β< 90° 0° <γ< 90°	a=1.5cm c=0.02cm Disc	8.6GHz	0.3%	75%	d=1.5m
Fig. 3		Horz.0°<β γ<20° Vert.70°<β γ<90° Ran.{0°<β<90° {20°<γ<90°	a=1.5cm c=0.02cm	8.6GHz	0.3%	75%	d=1.5m ε_g=4
Fig. 4.		0 <β<90° 0°<γ<90°	c=0.02cm a=0.75cm 1.5cm 3cm Disc	8.6GHz	0.3%	75%	d=1.5m ε_g=4
Fig 5		0 <β<90 0°<γ<90°	c=0.02cm a=1.5cm Disc	8.6GHz	0.3%	75% 50%	d=1.5m ε_g=4
Fig. 6	σ =1.73cm ℓ =30cm	0°<γ<90° 0°<β<180°	a=1.5cm c=0.02cm Disc	1.1GHz 4.25GHz 8.6GHz	0.3%	75%	d=1m ε_g=4
Fig. 7	kσ= 1. kℓ=12	0 <β<90 0°<γ<90°	l=1.3cm c=0.02cm Disc	4.5GHz	0.35%	65%	d=1m ε_g=25 & 3
Fig 8	kσ=0.1,05,0.9 kℓ=10	0 <β<90 0°<γ<90°	Rayleigh Sphere ω=0.3 τ=0.4				ε_g=18
Fig. 9 (a) (b), (c)	kσ =1, kℓ	0 <β<90 0°<γ<90°	a=1.3cm c=0.02cm Disc	4.5GHz	0.35%	65%	d=1m ε_g=25 & 3

Table 2

Parameter For Needle-Shaped Vegetation

Figures	Surface Parameters	β ,γ	A&C (cm) Shape	Freq. GHz	Vol. Fract. (%)	Plant Moist. (%)	Physical Depth d and Ground ε
Fig. 10		0 <β<90° 0°<γ<90°	a=0.17 c=3.066 Needle	4.5GHz	0.35%	20% 40% 80%	d=1m
Fig. 11		0° <β<90° 0° <γ<90	a=1.7 {c=1.5 {c=3.066 {c=6 Needle	4.5	0.35	65%	d=1.5m ε_g=5
Fig. 12	kσ=1 kℓ=10	0°<β, γ<10°	a=0.17 c=3.066 Needle	4.5	0.35	65%	d=1.5m ε_g=5
Fig. 13	kσ=1 kℓ=10	80°<β, γ<90°	a=0.17 c=3.066 Needle	4.5	0.35	65%	d=1.5m ε_g=5
Fig. 14	kσ=1 kℓ=10	35°<β, γ<55°	a=0.17 c=3.066 Needle	4.5	0.35	65%	d=1.5m ε_g=5
Fig. 15	kσ=1 kℓ=10	0°<β <90° 0°<γ<90°	a=0.17 c=3.066 Needle	4.5	0.35	65%	d=1.5m ε_g=5
Fig. 16		0°<β<90° 0°<γ<90°	{a=0.24 c=1.5 {a=0.17 c=3.066 {a=0.1 c=6cm Needle	4.5	0.35	65%	d=1.5m ε_g=5
Fig. 17		0°<β<90° 0°<γ<90°	{a=0.17 c=3.066 {a=0.17 c=6 Needle	4.5	0.35	65%	d=1.5m ε_g=5
Fig. 18		0° <β<90° 0° <γ<90°	a=0.17 c=3.06 Needle	1.5 GHz 4.5 GHz 10 GHz	0.35	65%	d=1.5m ε_g=5

LIST OF FIGURES

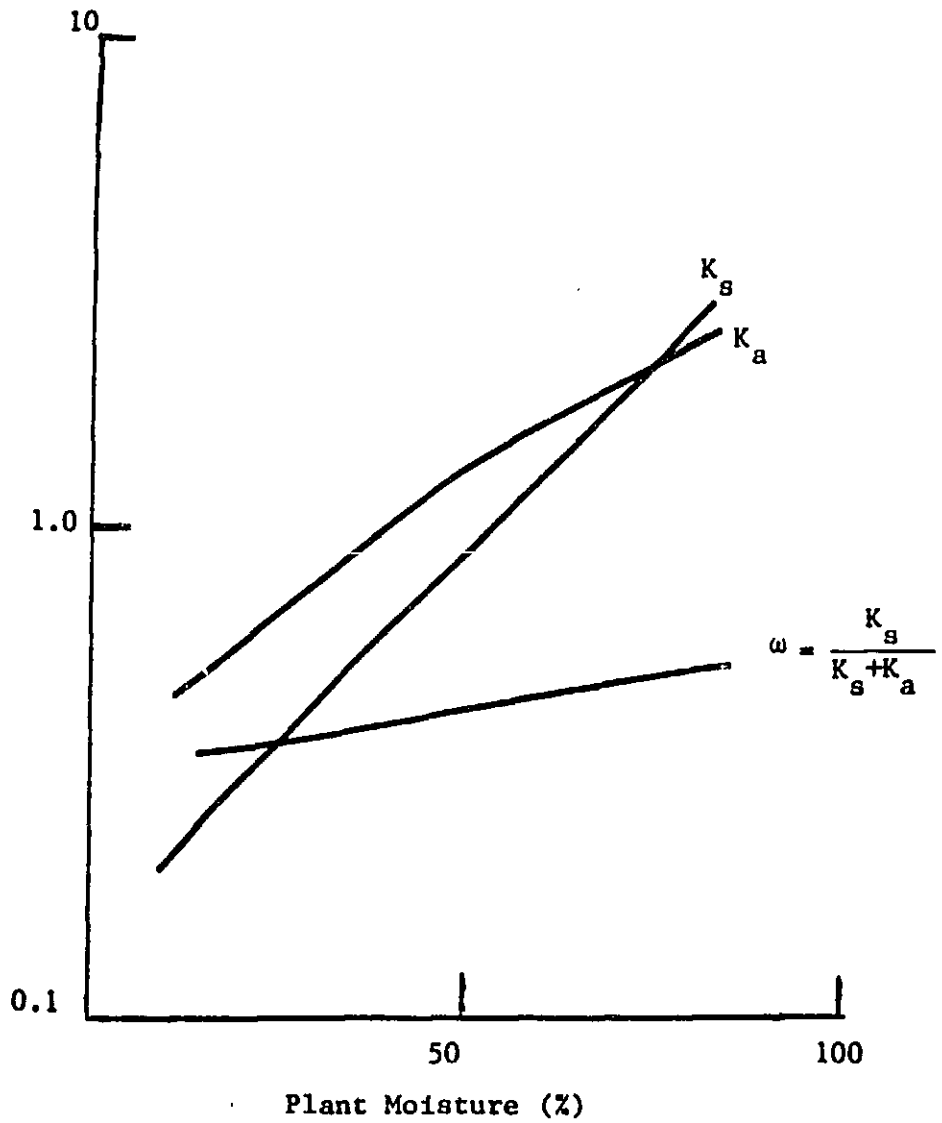

Figure 1. K_a, K_s, and ω versus plant moisture for a vegetation with disc-shaped leaves at 8.6 GHz.

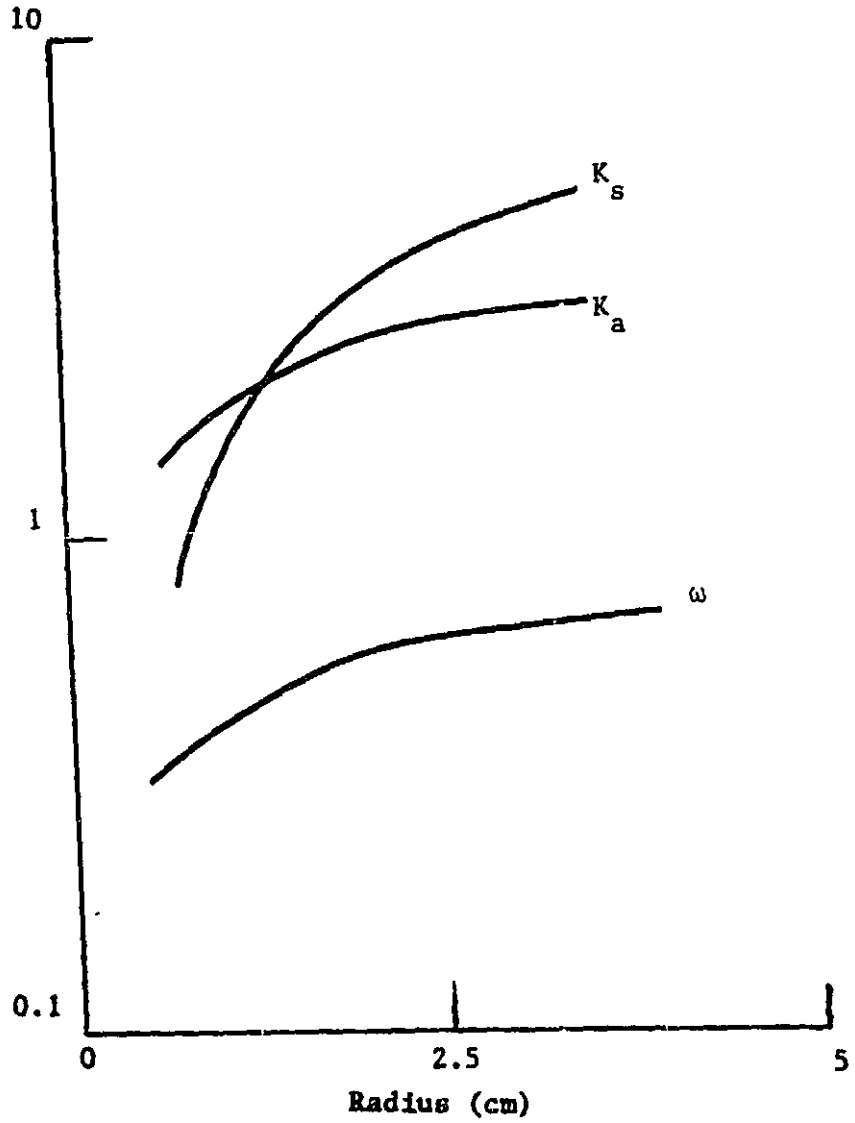

Figure 2. K_a, K_s, and ω versus the radius of the disc-shaped leaf.

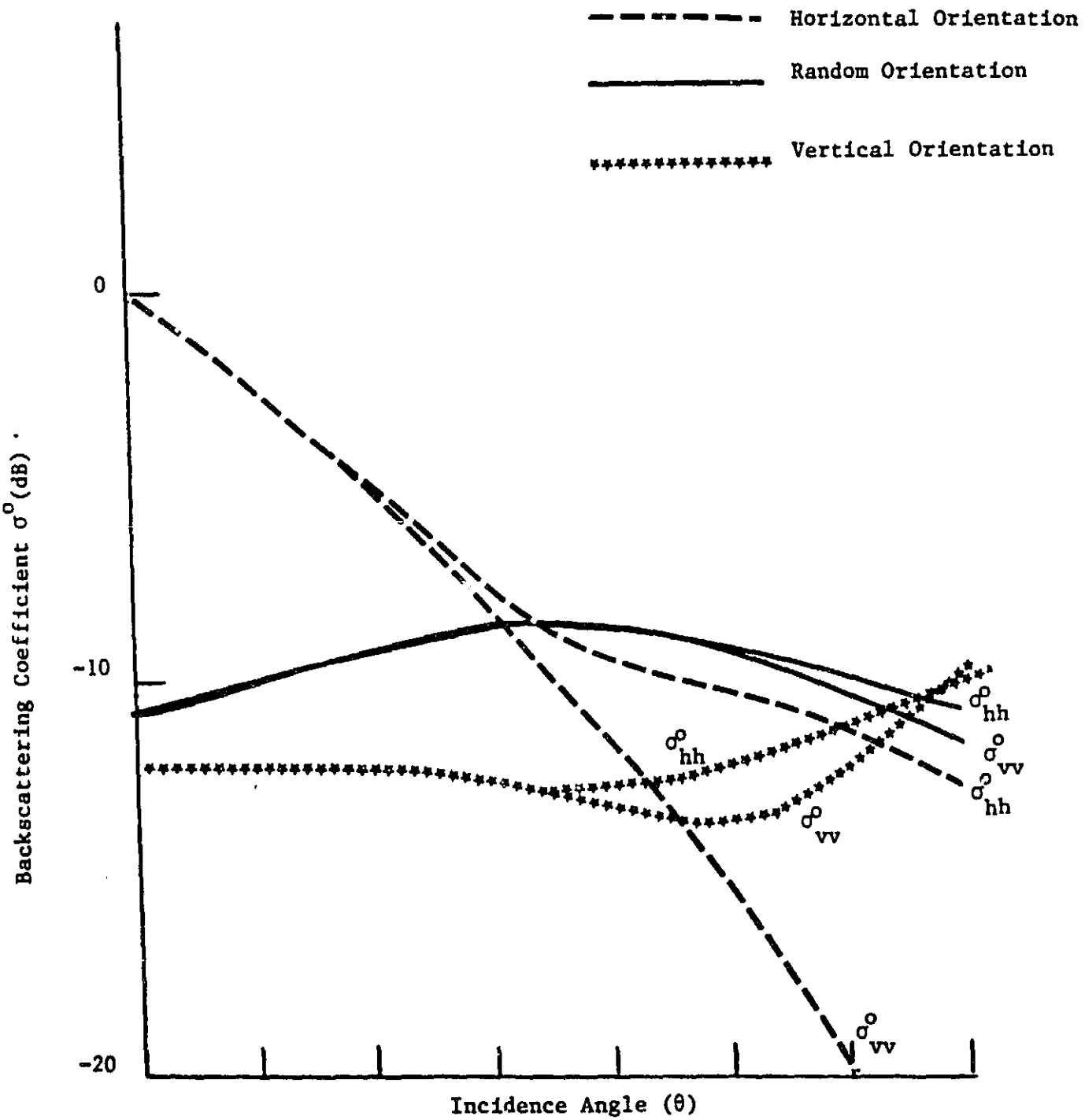

Figure 3. σ^{o}_{vv} and σ^{o}_{hh} versus the incidence angle θ. Three different leaf angular distributions are shown: vertical ($70^{o} < \gamma, \beta < 90^{o}$), horizontal ($0^{o} < \gamma, \beta < 20^{o}$), and random ($0^{o} < \gamma, \beta < 90^{o}$).

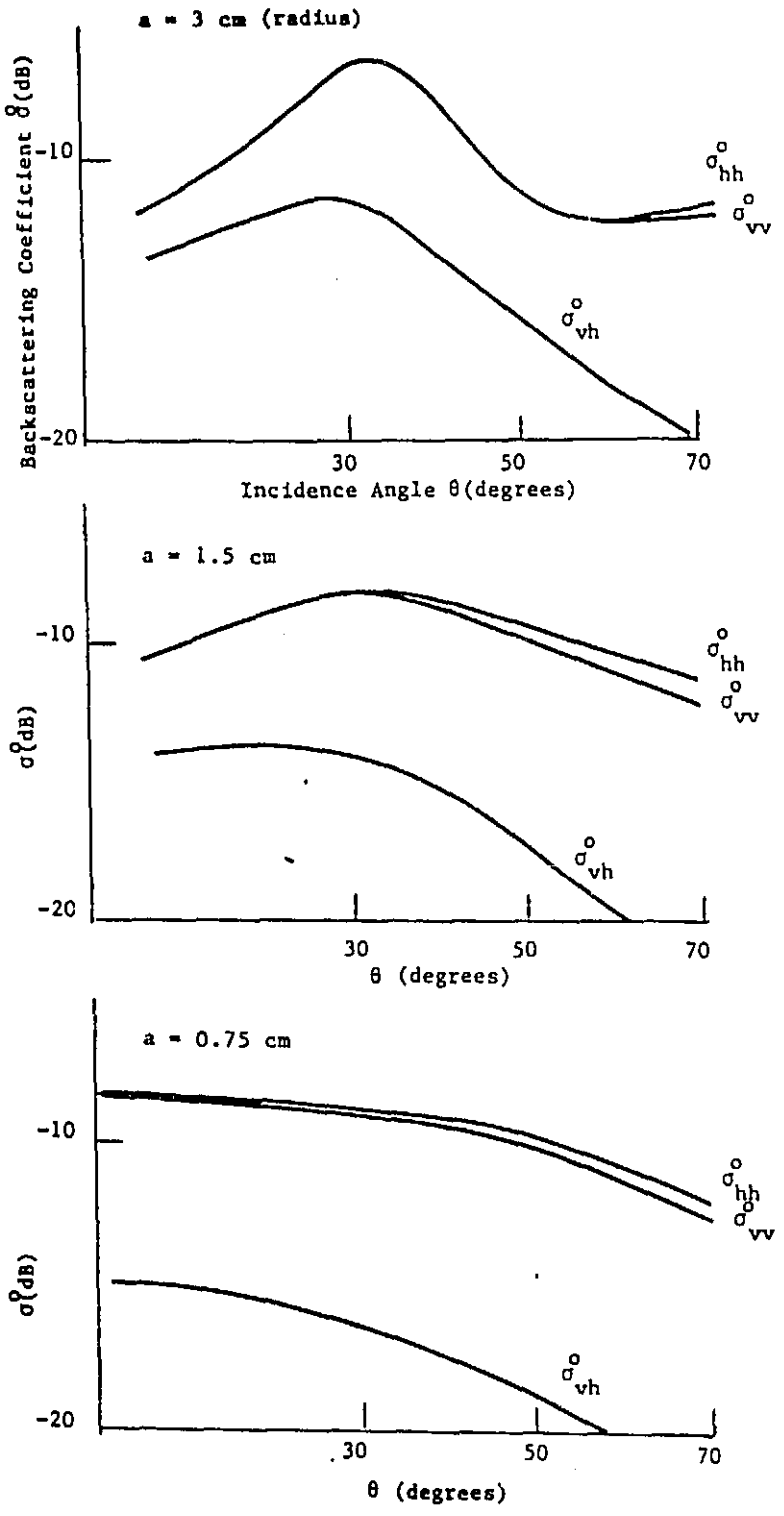

Figure 4. Effects of change in the radius of the leaf on the back scattering coefficients σ^o_{vv}, σ^o_{hh}, and σ^o_{hh}.

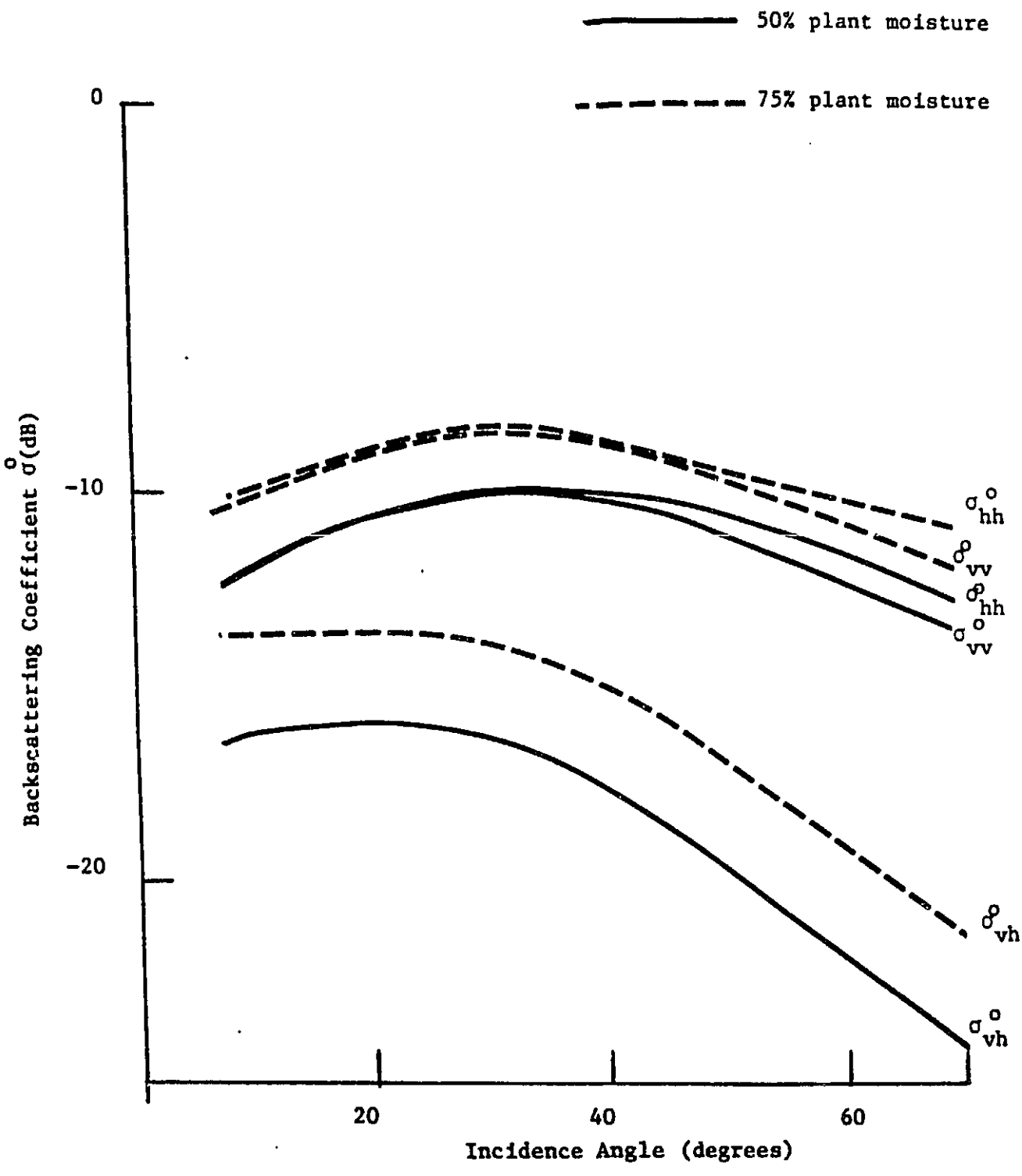

Figure 5. Effects of change in the plant moisture on the backscattering coefficients σ^{o}_{vv}, σ^{o}_{hh}, and σ^{o}_{vh}.

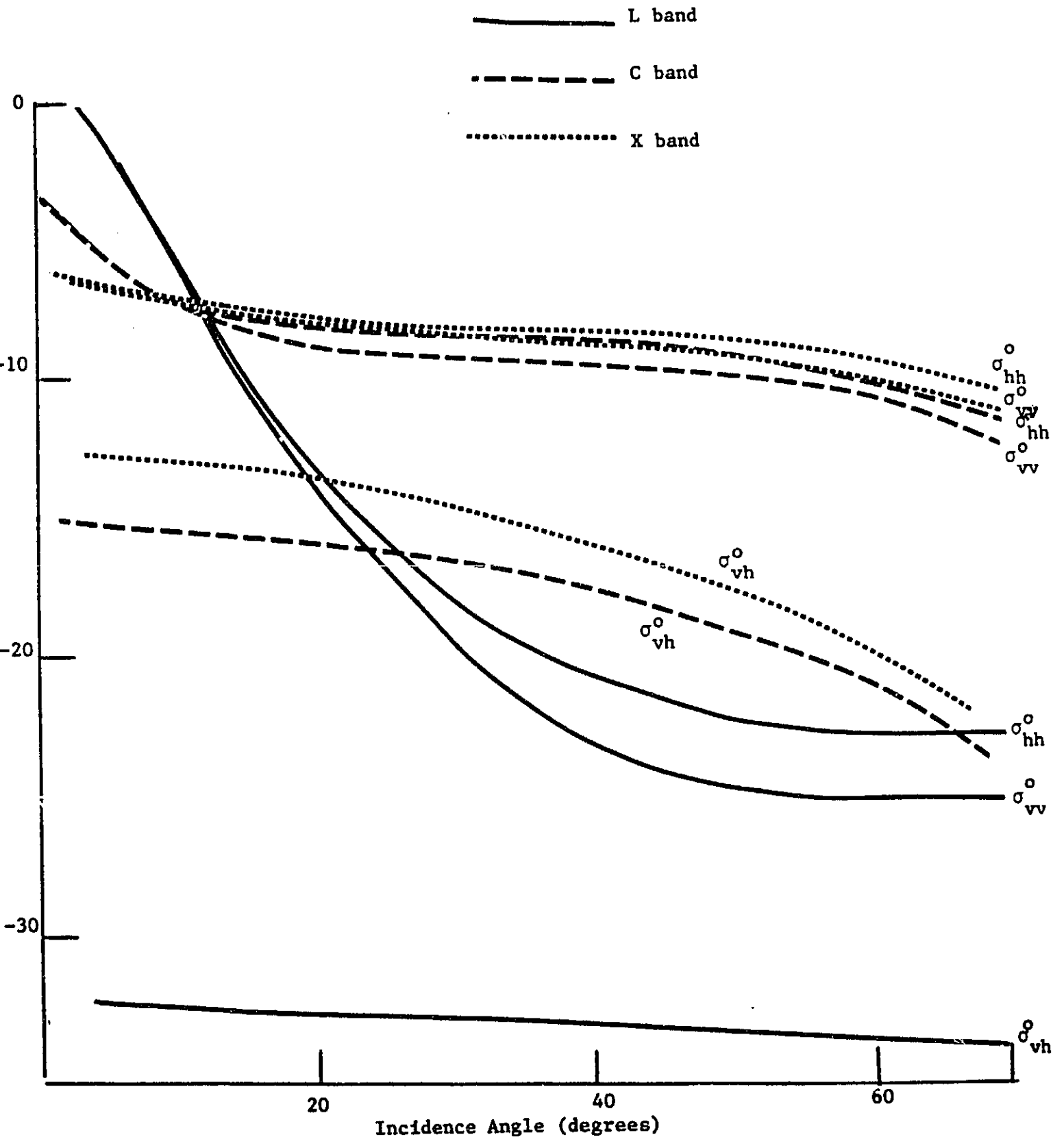

Figure 6. Effects of change in frequency on the backscattering coefficients σ^o_{vv}, σ^o_{hh}, and σ^o_{vh}. Frequencies considered are at L, C, and X bands.

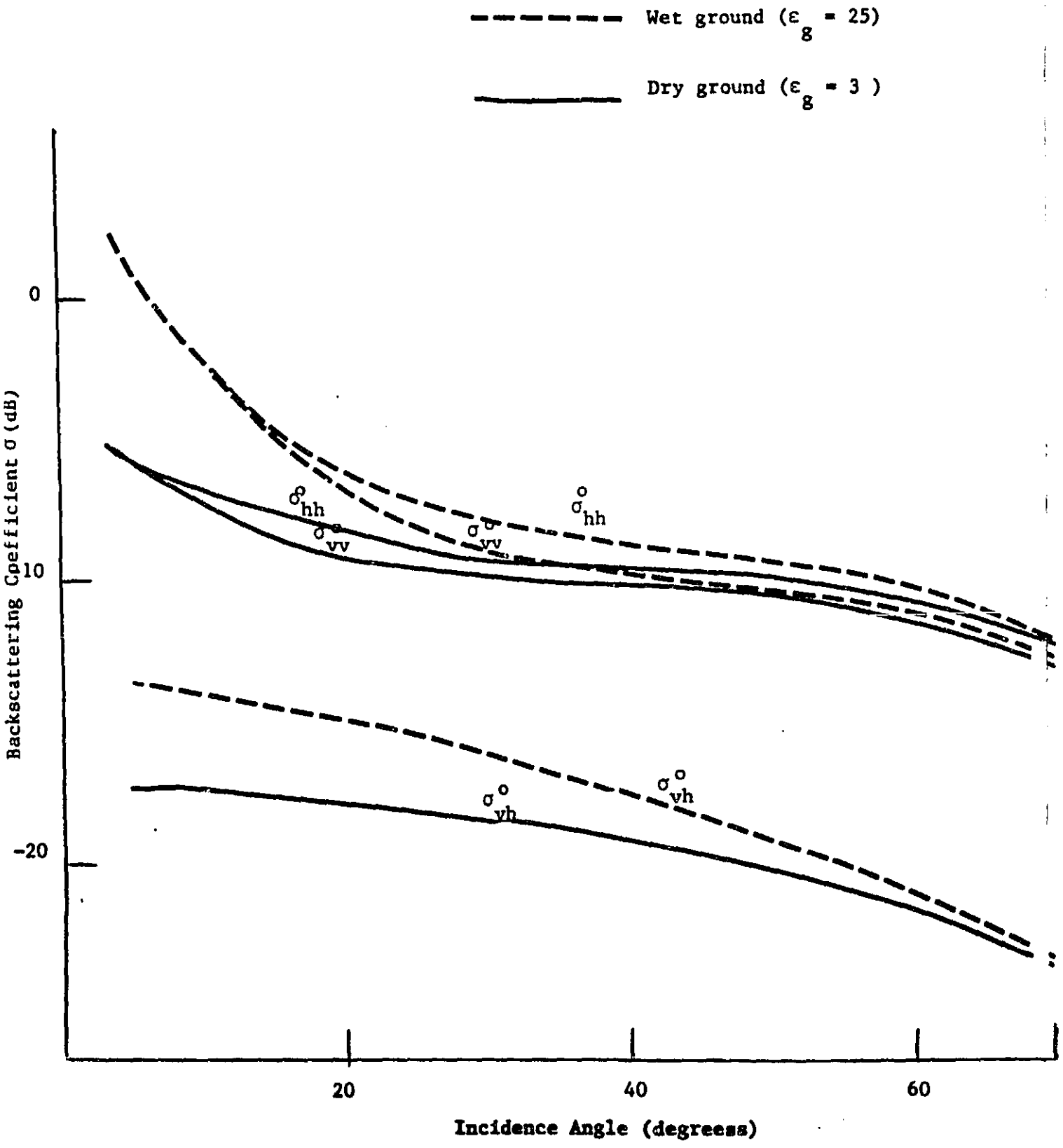

Figure 7. Effects of change in ground permittivity on the backscattering coefficients σ^o_{vv}, σ^o_{hh}, and σ^o_{vh}.

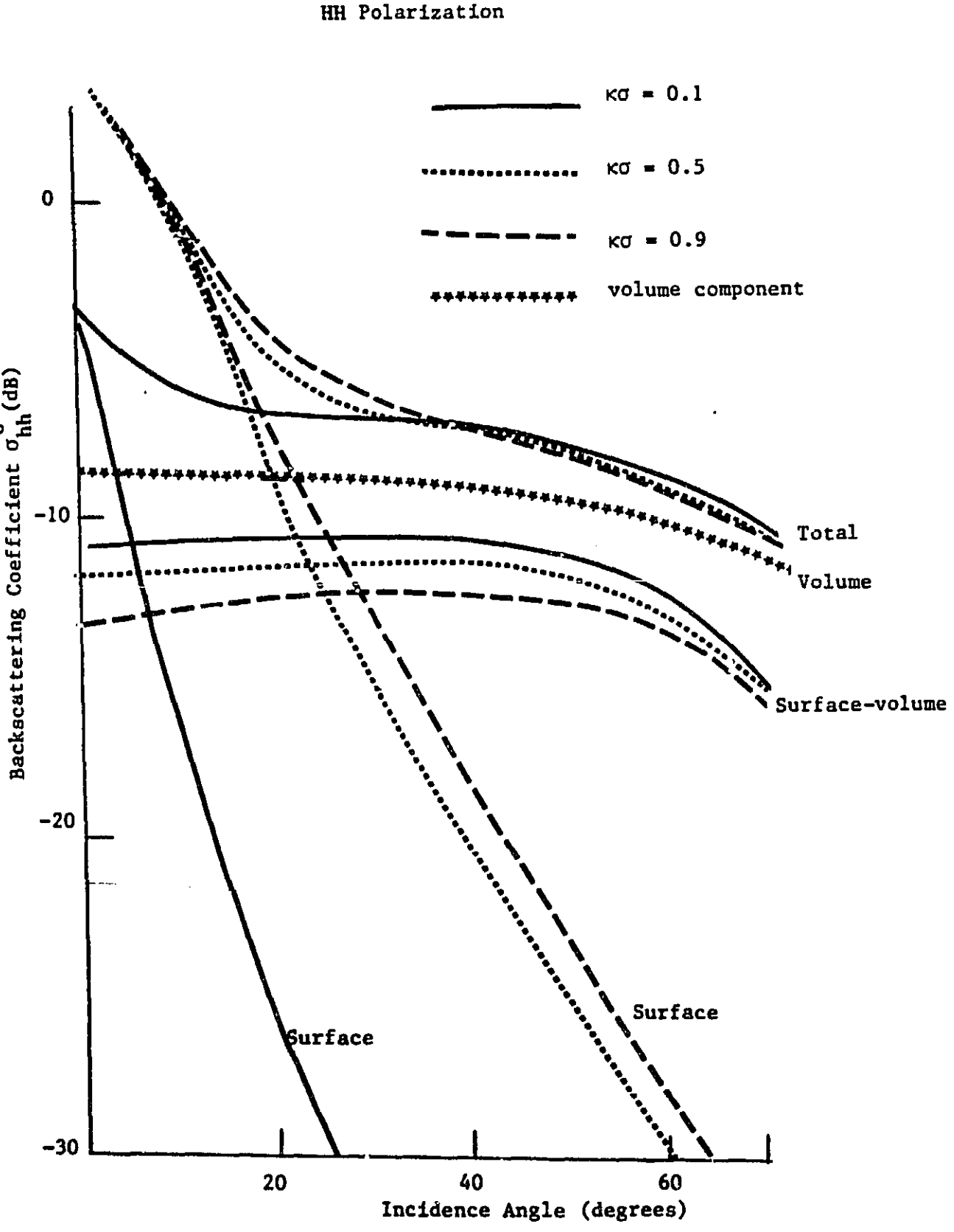

Figure 8. Effects of change in kσ on backscattering coefficient σ^{o}_{hh}. Contributions due to surface-, volume-, and surface-volume scattering to total backscattering are shown separately.

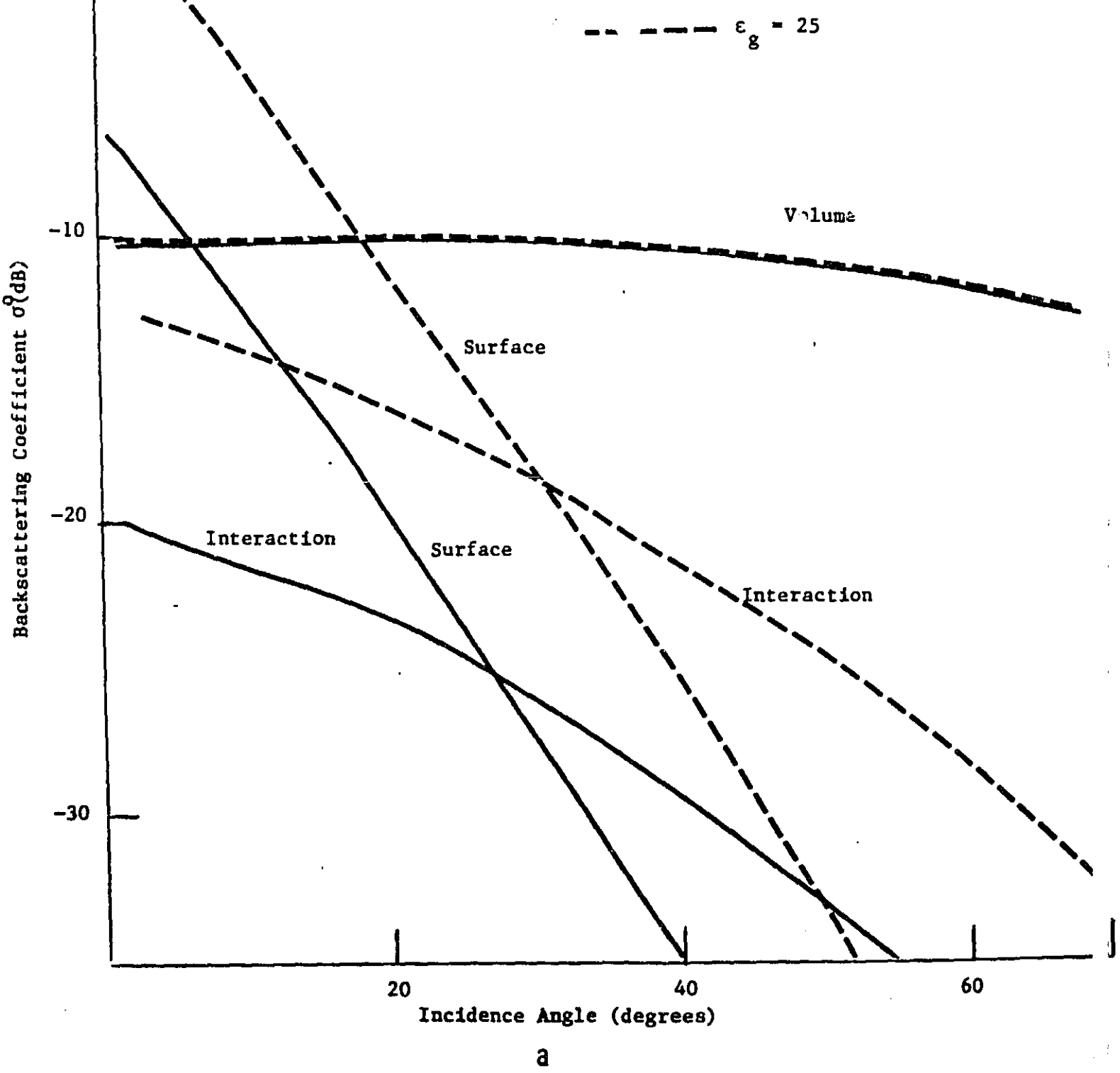

Figure 9. Comparisons between the relative contributions of surface, volume, and surface-volume interaction scattering terms for (a) VV polarization, (b) HH polarization, and (c) VH polarization.

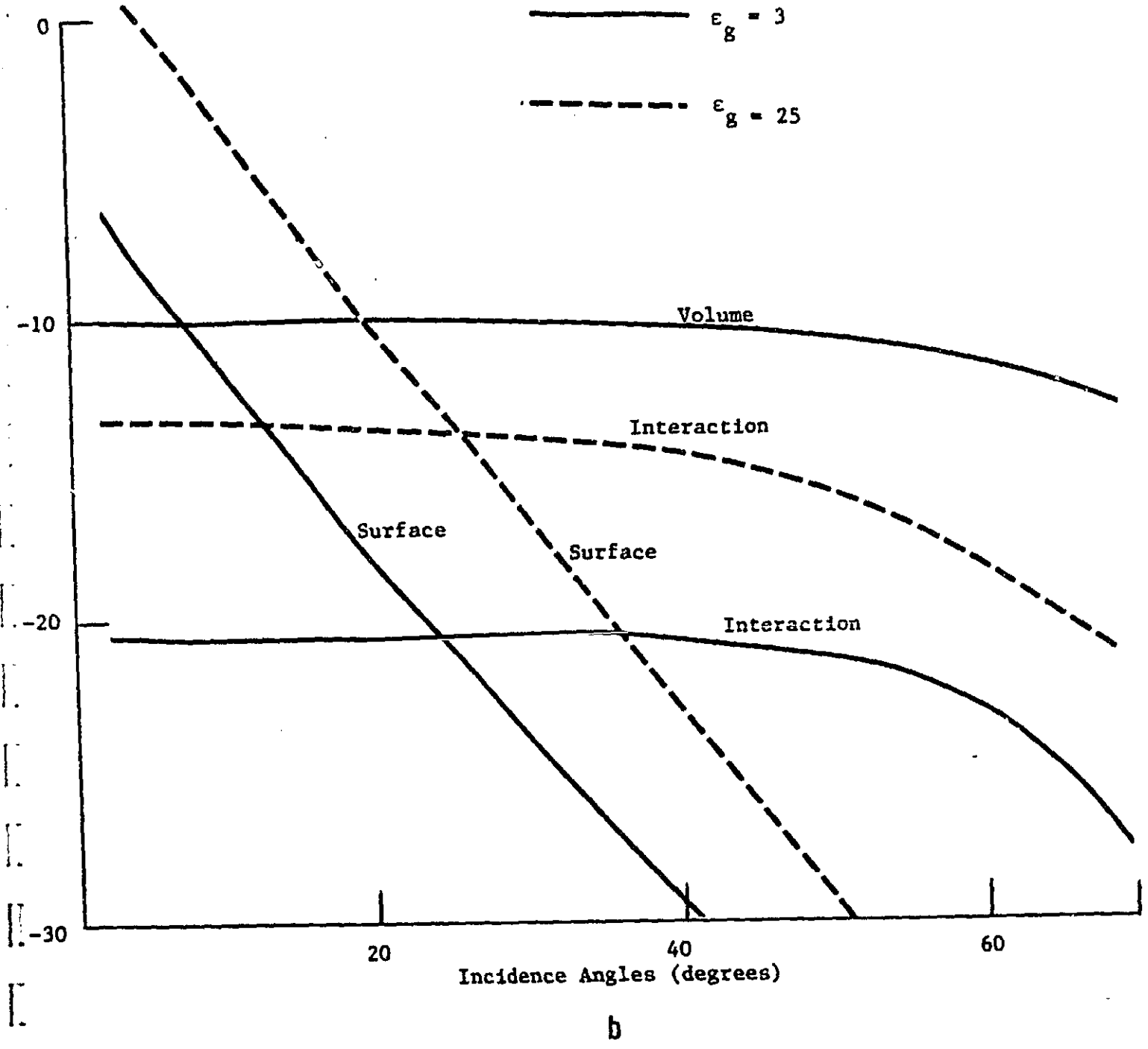
$\varepsilon_g = 3$
$\varepsilon_g = 25$
0
-10
-20
-30
Volume
Interaction
Surface
Surface
Interaction
Backscattering Coefficient σ(dB)
20
40
60
Incidence Angles (degrees)

b

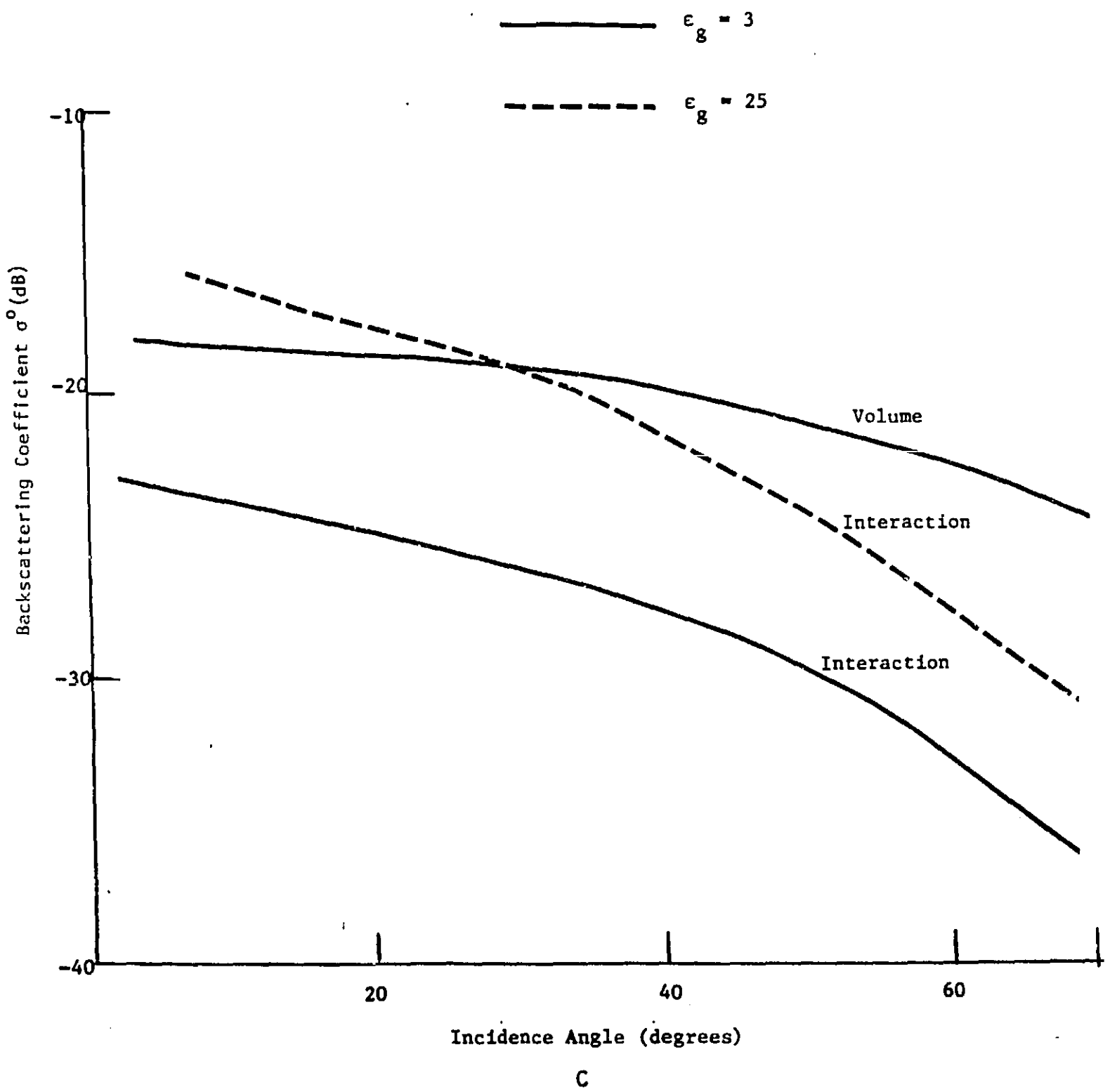
ϵ_g = 3
ϵ_g = 25
-10
-20
-30
-40
Backscattering Coefficient σ^o(dB)
Volume
Interaction
Interaction
20
40
60
Incidence Angle (degrees)

C

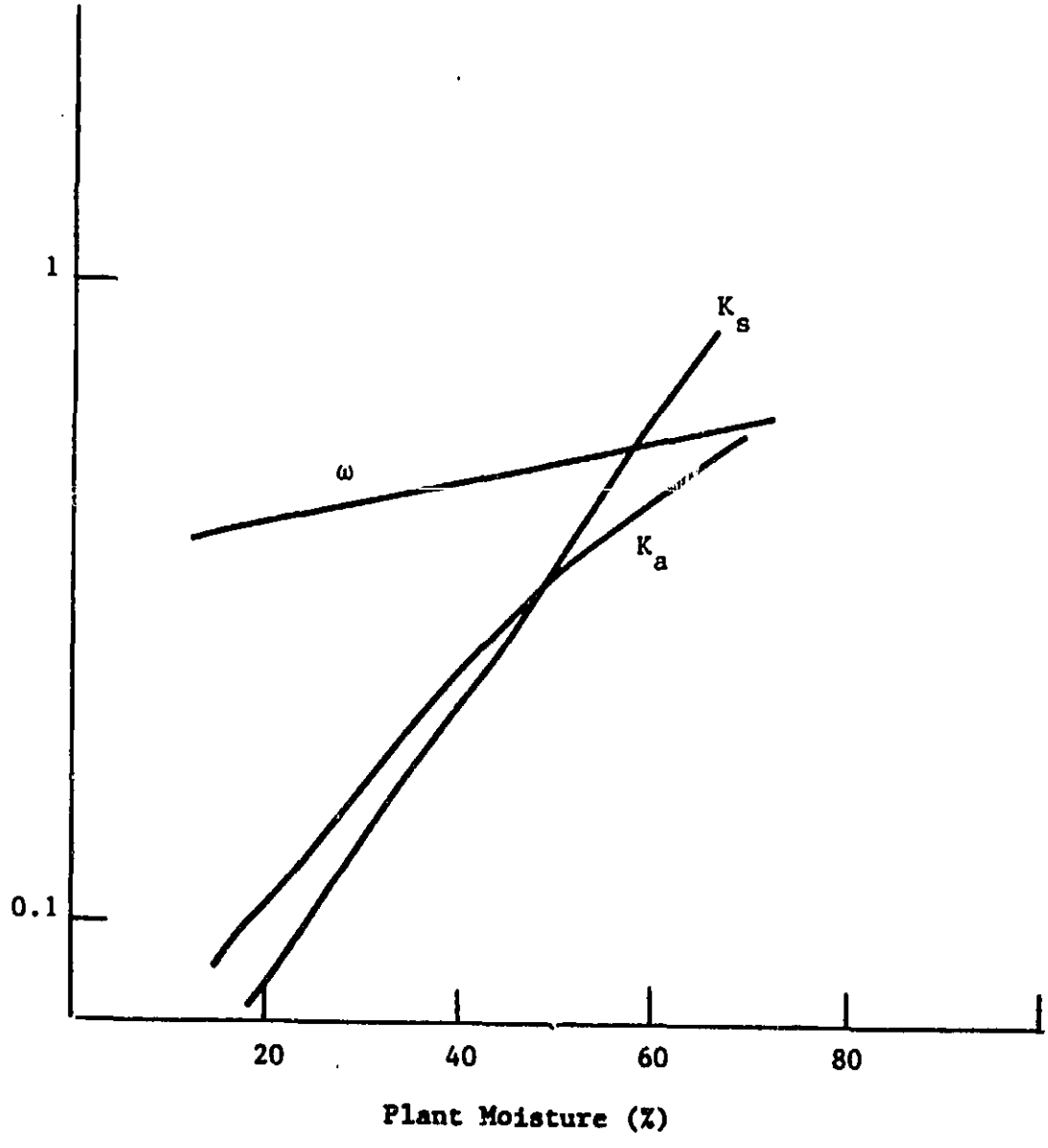

Figure 10. K_a, K_s, and ω versus plant moisture for a needle-shaped vegetation at 4.5 GHz.

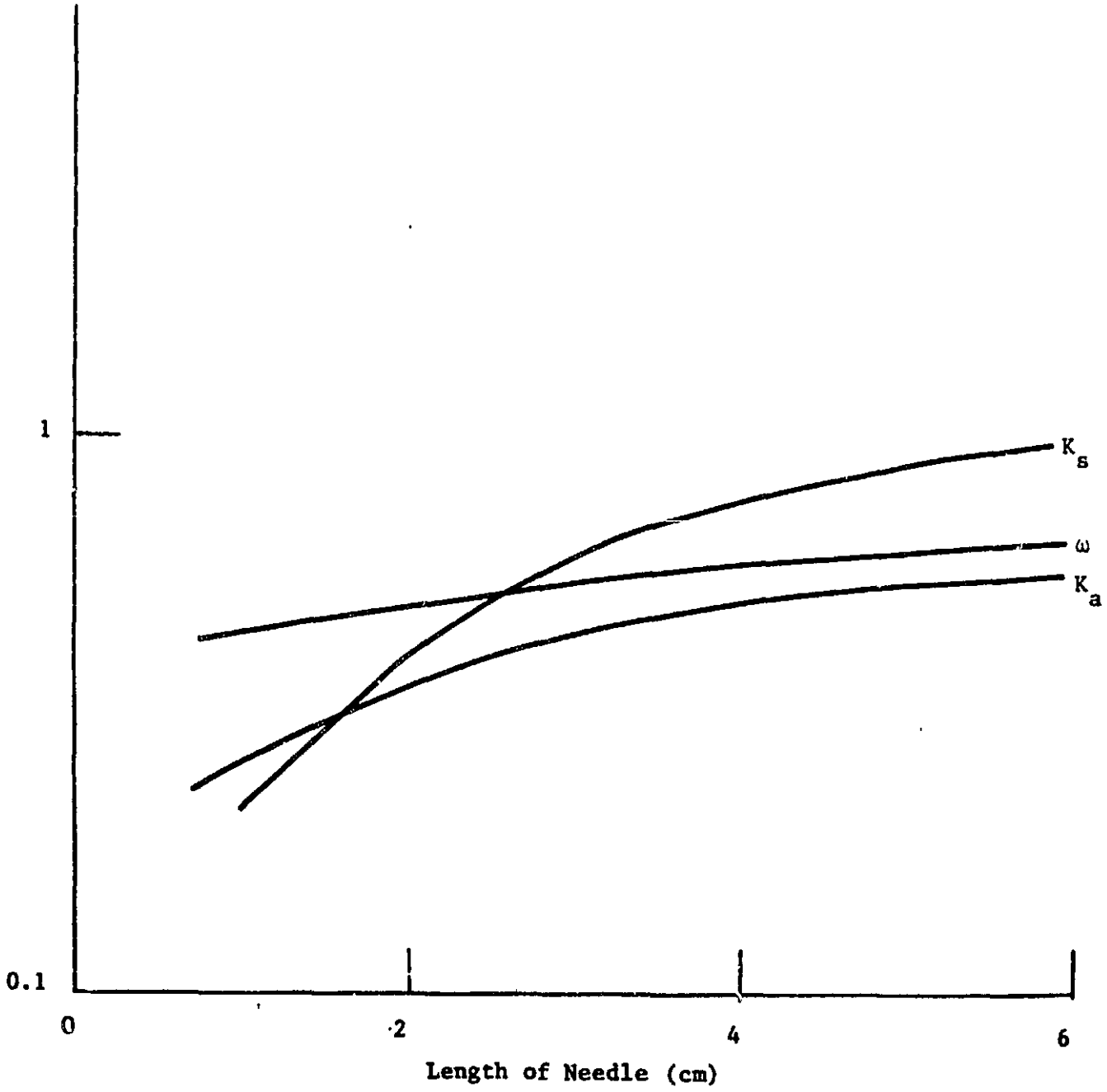

Figure 11. K_a, K_s, and ω versus the length of the needle-shaped leaf at 4.5 GHz.

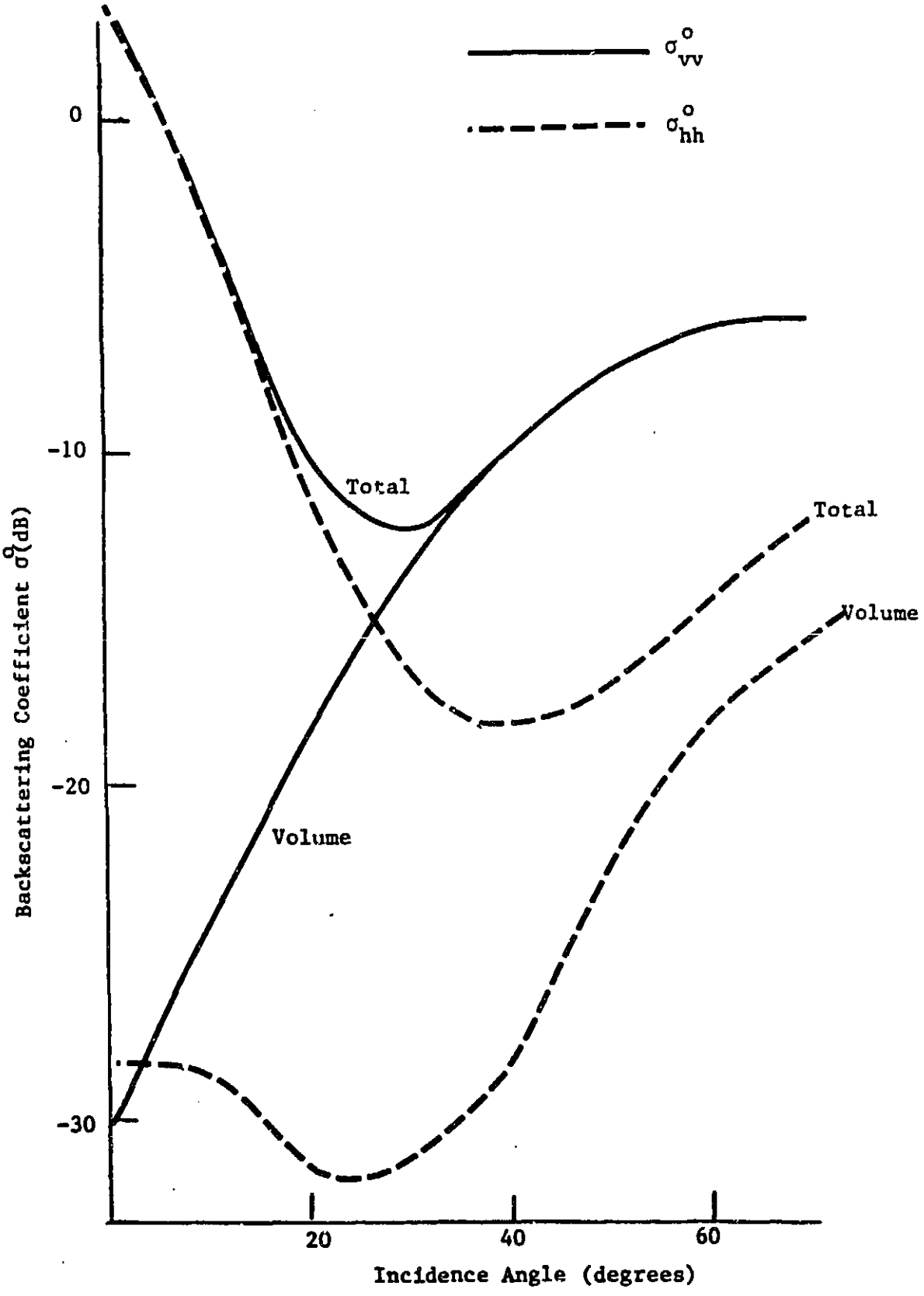
σ^o_{vv}
σ^o_{hh}
0
-10
-20
-30
Total
Total
Volume
Volume
Backscattering Coefficient σ^o(dB)
20
40
60
Incidence Angle (degrees)

Figure 12.

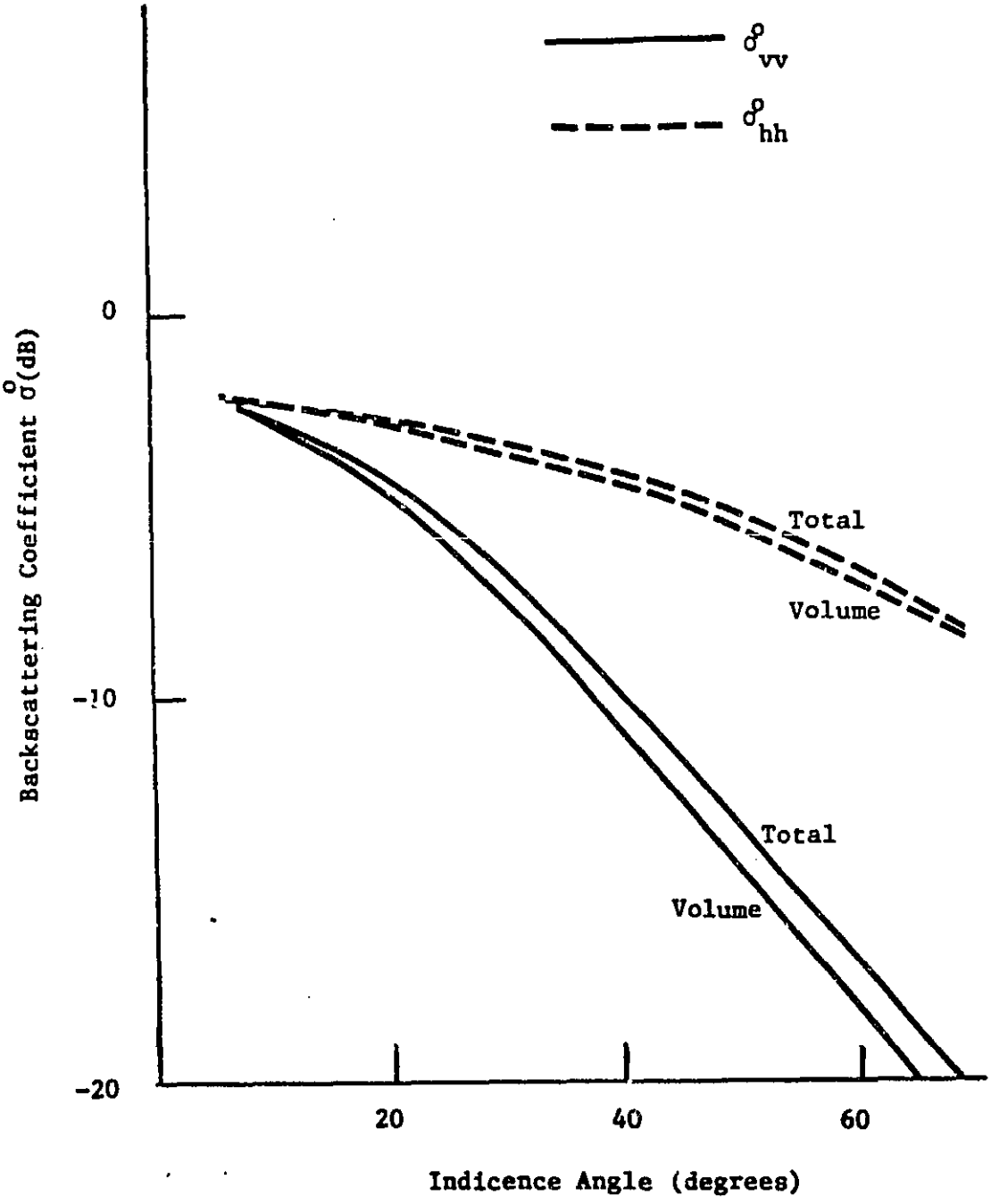
σ^o_{vv}
σ^o_{hh}
0
-10
-20
Backscattering Coefficient σ^o(dB)
Total
Volume
Total
Volume
20
40
60
Indicence Angle (degrees)

Figure 13.

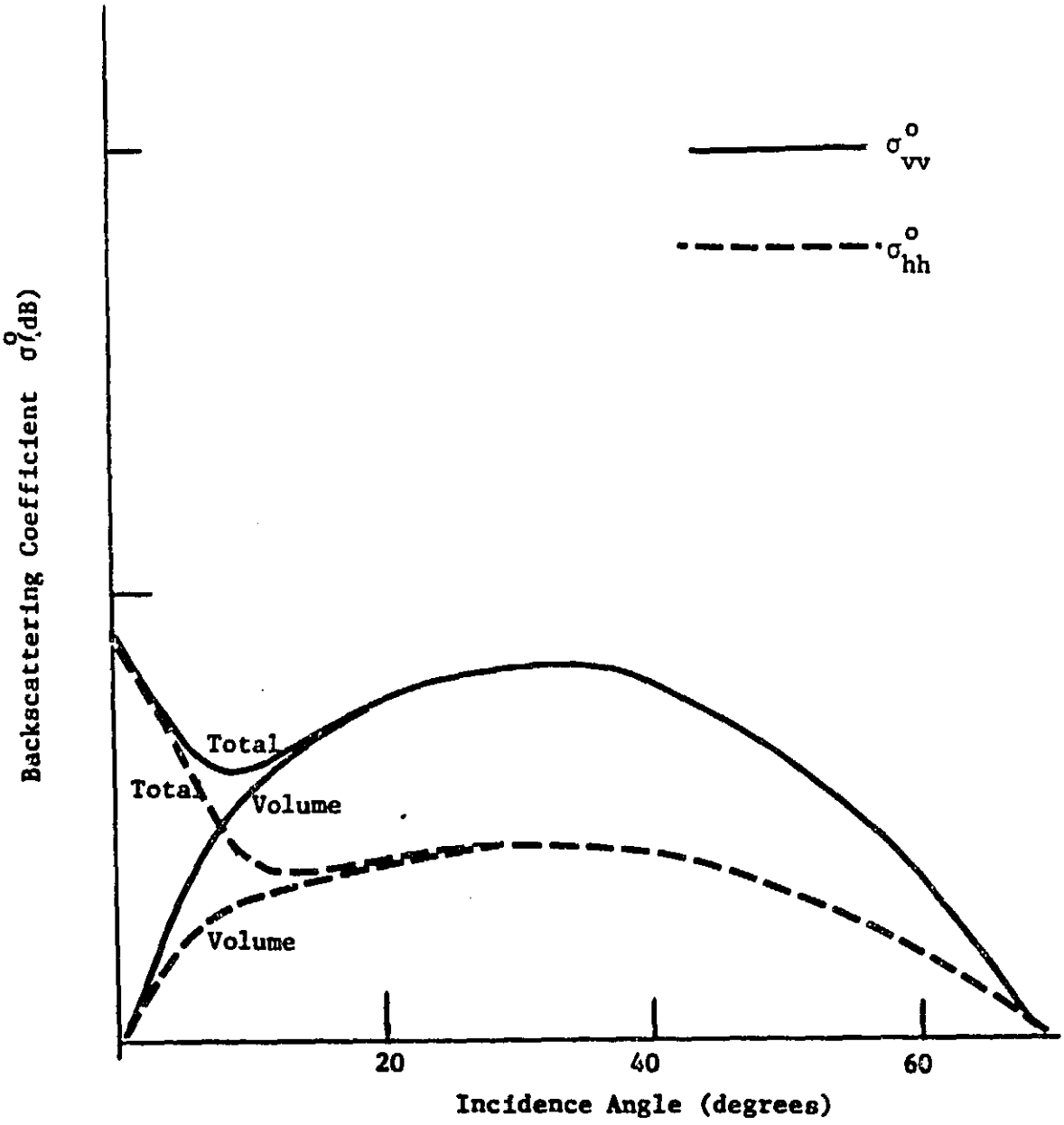
σ^o_{vv}
σ^o_{hh}
Backscattering Coefficient σ^o (dB)
Total
Total
Volume
Volume
20
40
60
Incidence Angle (degrees)

Figure 14.

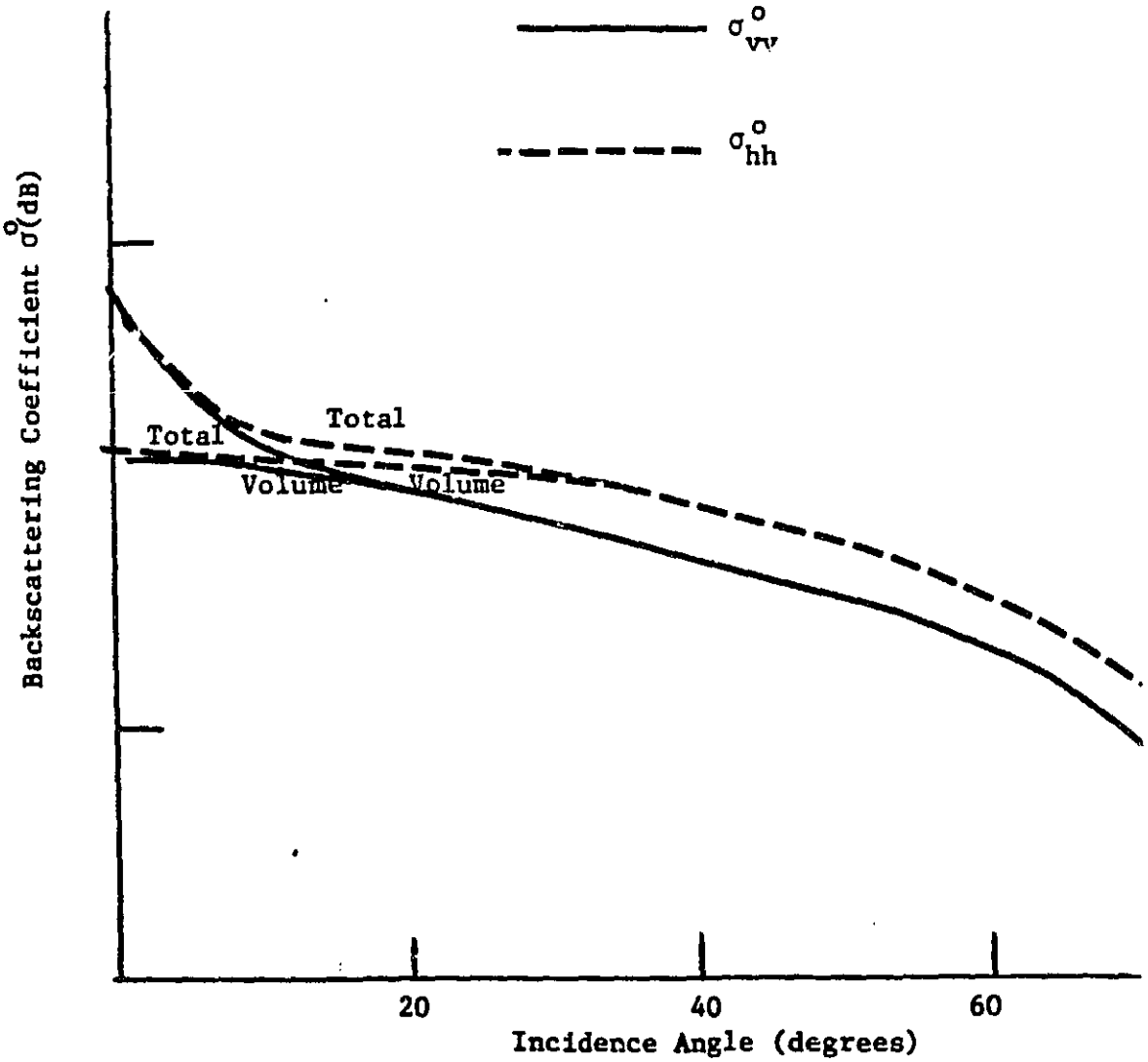
σ^o_{vv}
σ^o_{hh}
Backscattering Coefficient σ^o(dB)
Total
Total
Volume
Volume
20
40
60
Incidence Angle (degrees)

Figure 15.

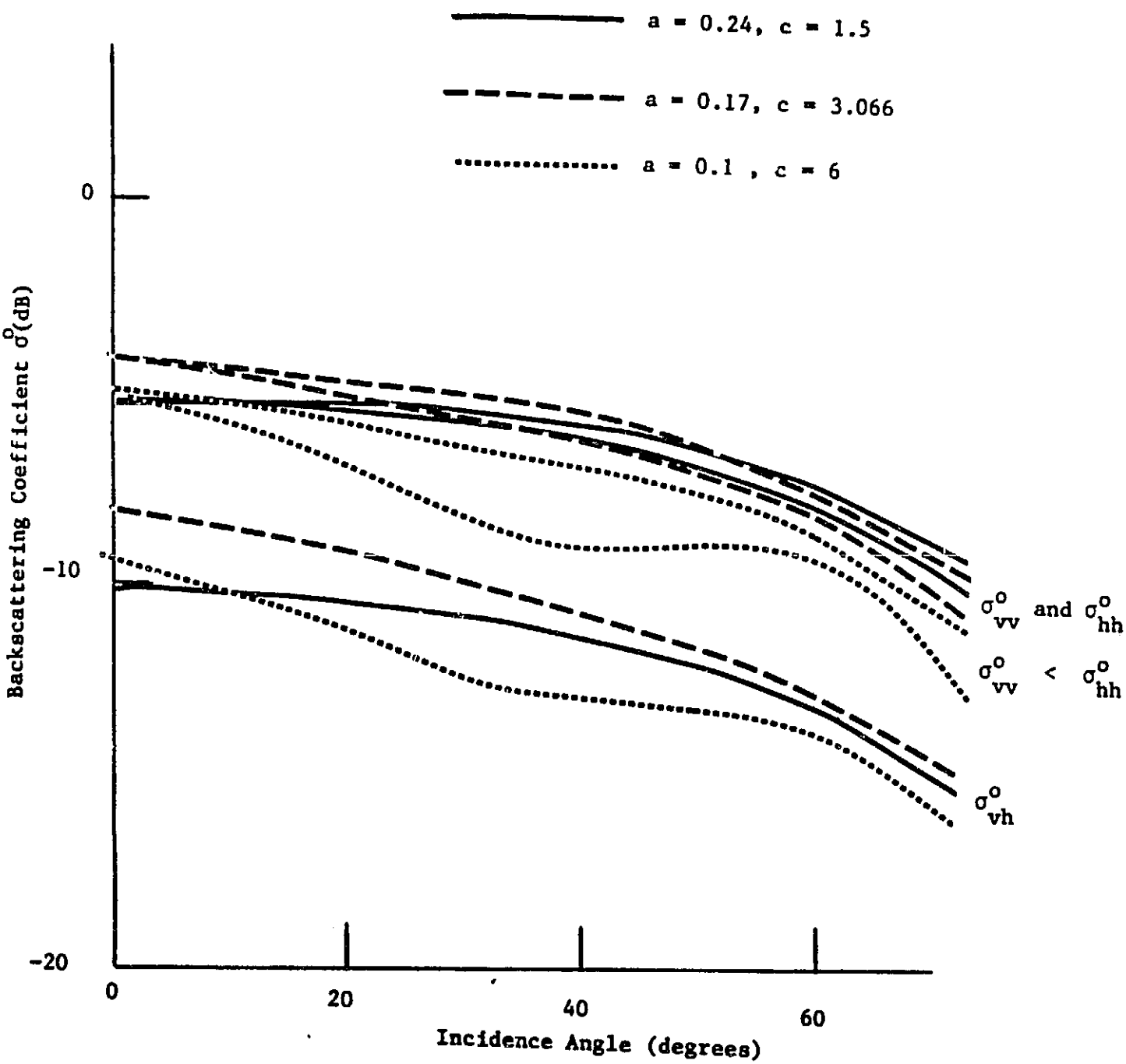
a = 0.24, c = 1.5
a = 0.17, c = 3.066
a = 0.1 , c = 6
0
-10
-20
Backscattering Coefficient σ°(dB)
σ°vv and σ°hh
σ°vv < σ°hh
σ°vh
0
20
40
60
Incidence Angle (degrees)

Figure 16.

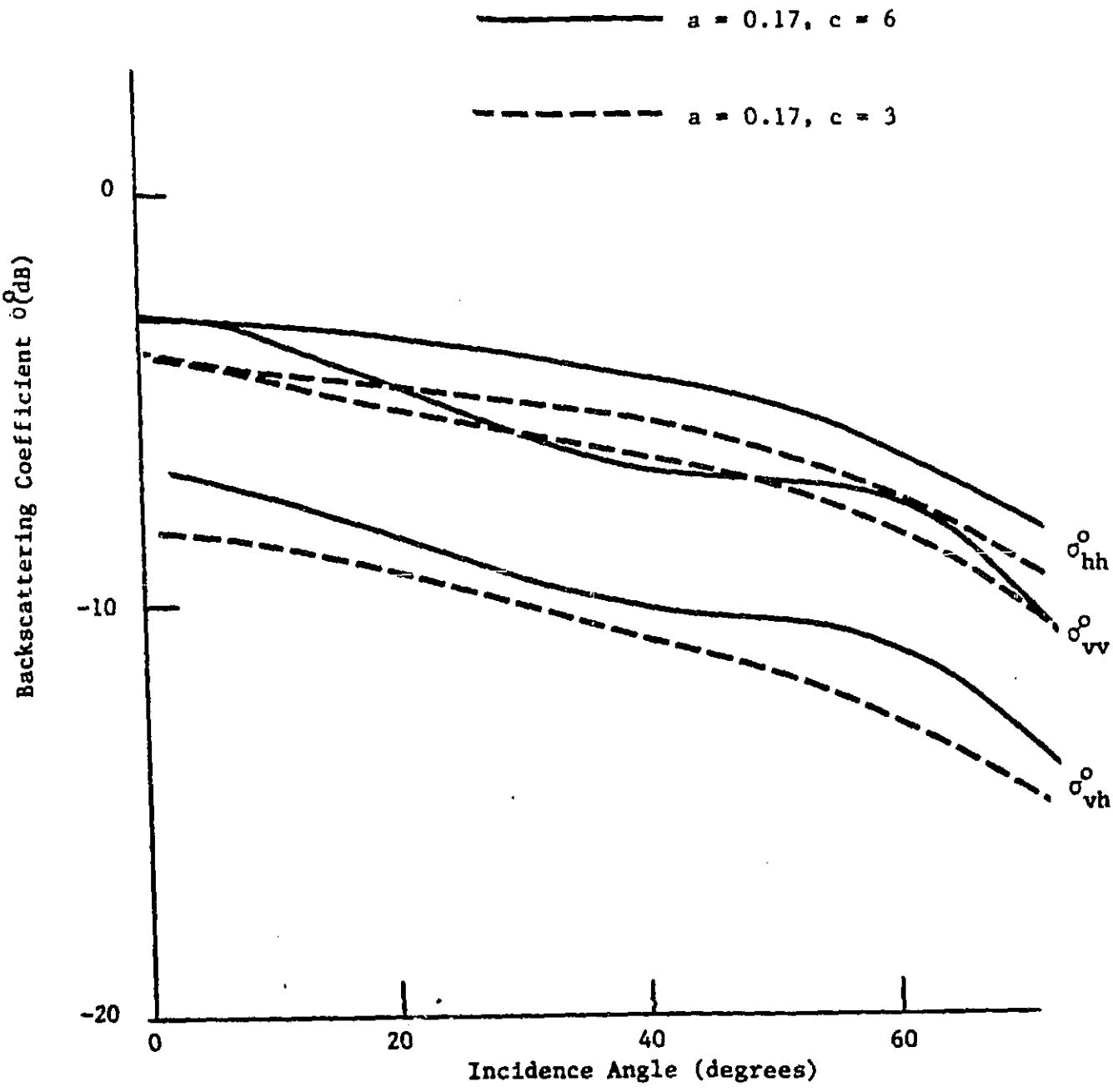
a = 0.17, c = 6
a = 0.17, c = 3
0
-10
-20
Backscattering Coefficient σ°(dB)
σ°hh
σ°vv
σ°vh
0
20
40
60
Incidence Angle (degrees)

Figure 17.

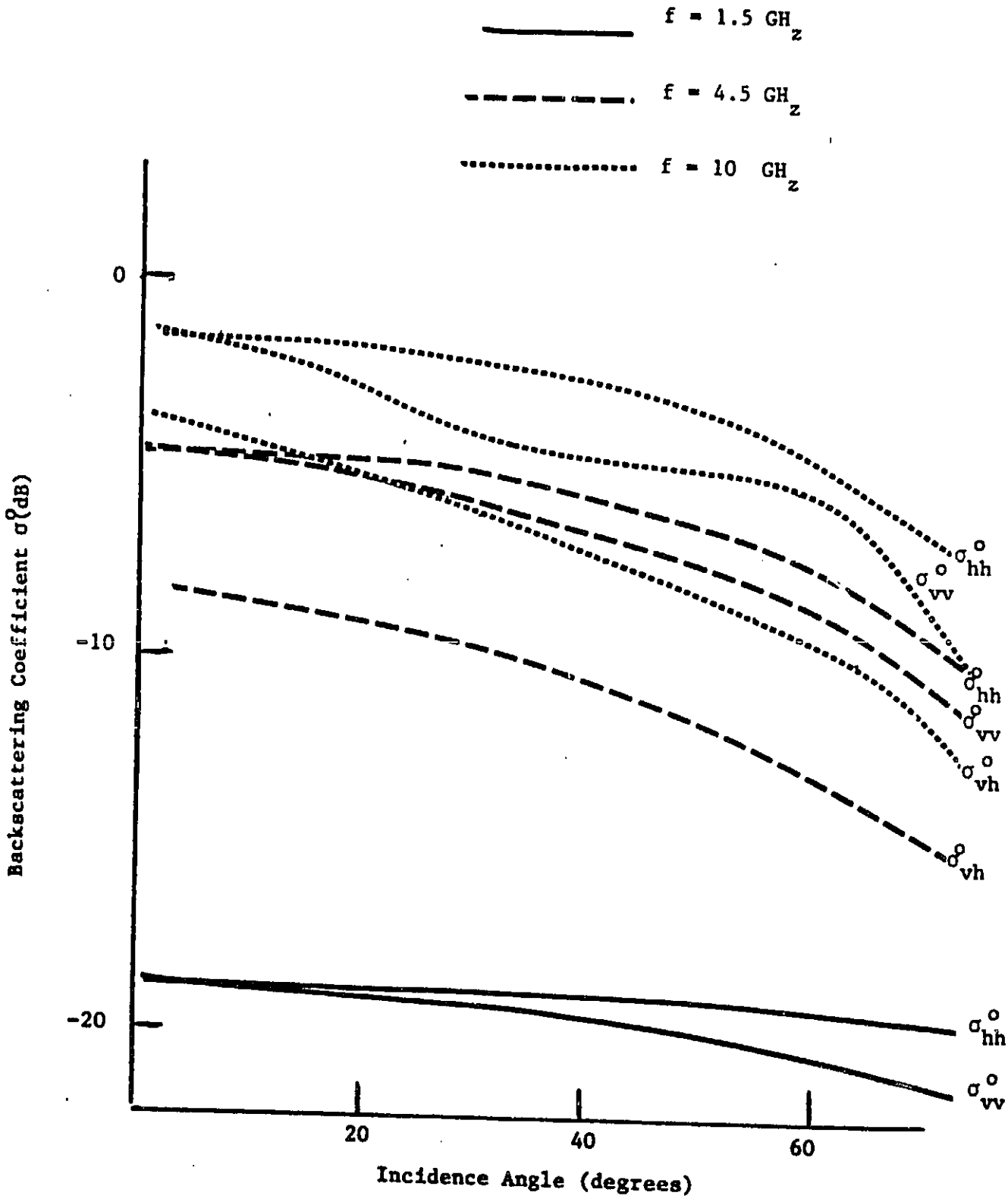
f = 1.5 GHz
f = 4.5 GHz
f = 10 GHz
0
-10
-20
Backscattering Coefficient σ°(dB)
σ°hh
σ°vv
σ°hh
σ°vv
σ°vh
σ°vh
σ°hh
σ°vv
20
40
60
Incidence Angle (degrees)

Figure 18.